Quantitative Analysis of Cell-Surface Interactions and Cell Adhesion Process in Real-time

A Thesis

Submitted to the Faculty

of

Drexel University

by

Soonjin Hong

in partial fulfillment of the

requirements for the degree of

Doctor of Philosophy

April 2008

ACKNOWLEDGEMENTS

I would like to express my gratitude to many people for the precious and continuous help and guidance. Without them, I would not be able to accomplish my Ph.D.

First of all, I'd like to thank to my adviser, Dr. Kenneth A. Barbee. His knowledgeable advice and suggestion guided me to fruitful results and made it possible to do the comprehensive research. I was able to learn how to plan and conduct the in-depth research, which will be a great asset to my future career. Especially, I thank him for his humane attitude to understand a student's situation.

I am also very grateful to committee members, Drs. Lec, Allen, Marcolongo and Reginato, for their technical and academic advice. Their comments and feedbacks were valuable in refining the thesis. Dr. Lec gave me continuous advice on the sensor system. Dr. Marcolongo kindly allowed me to use her experimental apparatus and Dr. Reginato generously provided me with cells and valuable suggestions on the experiments.

I appreciate to all my friends in Dr. Barbee's and Dr. Lec's lab and I would like to remind the friendship with Dihui Hong, Devrim Kilinc, Allison Andrews, Ertan Ergezen, Robert Hart and Dr. Dianne Rothstein. Lastly, I would like to give my special thanks to my wife and children; Kyungcho, Alex, Hannah, Andrew and Emily.

TABLE OF CONTENTS

LIST OF TABLES

LIST OF FIGURES

ABSTRACT

Quantitative Analysis of Cell-Surface Interactions and Cell Adhesion Process in Real-time

Soonjin Hong

Kenneth A. Barbee, Ph.D.

The cell adhesion process and cellular interactions with extracellular matrix (ECM) proteins were quantitatively evaluated using a thickness shear mode (TSM) sensor. For understanding cell-surface interactions, specific effects of receptor-mediated adhesion, the glycocalyx, and surface charge on initial cell-surface attachment and steady state adhesion of bovine aortic endothelial cells (BAECs) were investigated. The result showed that integrin binding determines the kinetics of initial cell attachment while heparan sulfate proteoglycan (HSPG) modulates steady state adhesion strength. Coating the sensor surface with the positively charged poly-D-lysine (PDL) enhanced the initial interaction with substratum. In order to relate sensor data to the adhesion of the cells, we performed independent measures of cell spreading and adhesion strength. The adhesive interactions of human mammary epithelial cells, MCF-10A, with a fibronectin coated sensor were altered by overexpressing Her2/Neu oncogene and by blocking integrin function with soluble GRGDS. Correlation of ΔR with cell spreading and adhesion measurements revealed three phases: adhesion, spreading and structural reorganization. In the initial adhesion phase, ΔR increases rapidly as the cells bind to the substratum and began to flatten. The rate of change of ΔR is proportional to the adhesion strength. As the cells spread beyond their initial projected area, ΔR increased in proportion to the change in area. In the final phase, as the cells approach their final spread area, further increases in ΔR reflect structural changes, possibly indicating maturation of cytoskeleton and focal adhesion formation. In order to see the effect of cell deformability on the initial adhesion, the elastic modulus of spherical cells were evaluated. The calculation of Young's moduli showed that oncogene expressing cells were more compliant than normal cells (1.09kPa±0.36 vs. 2.95kPa±0.34), which was reflected to the initial increase of ΔR. The real time monitoring capability of this technique with high temporal resolution provides more detailed information on the kinetics of the different stages of the adhesion process. The analysis of adhesion properties of normal versus transformed mammary epithelia correlates with changes in integrin expression, demonstrating the usefulness of TSM sensor measurement system for understanding adhesion characteristics in real time as it relates to phenotypic variations.

CHAPTER 1

BACKGROUNDS

1.1 Cell adhesion mediated by complex intracellular and extracellular events

Cell adhesion has been of particular interest because it plays important roles in the regulation of cell behavior in wound healing and tissue regeneration, such as the regulation of growth, differentiation, migration and survival of cells. Cell adhesion is the integrated process of multiple complex events, such as specific binding of membrane proteins with extracellular matrix (ECM), intracellular cytoskeleton (CSK) formation and the signal transduction. These events are strictly controlled by complicated mechanisms and are highly interconnected and interdependent. This continuous and complex cell adhesion process is driven by ligand-receptor interactions, especially integrin bindings [1]. Heterodimeric transmembrane integrin receptors recognize ECM ligands, such as fibronectin (FN), vitronectin (VN), laminin (LN) and collagen. Besides the physical connection, integrin binding relays signals from ECM, which invoke several subsequential events [2, 3]. Based on integrin binding, cells develop the intracellular cytoskeleton network, which is the polymeric network of structural filaments including actin, intermediate filament and microtubule. Especially, the cell shape and structure are determined by the actin filament formation influenced by signaling by growth factor receptors and intregrin binding. Actin filament network is physically connected to ECM proteins through clusters of integrins. During the dynamic cell adhesion process cells actively modulate cell-ECM interactions and the extracellular signaling by reorganizing the ECM, rearranging fibrillar components or even secreting the new proteins [4].

1.2 Multi-functional integrin and intrinsic adhesivity of cells

As a major family of cell surface receptors, integrins provide physical contacts and signaling pathways with surrounding environment. Integrins consist of two non-covalently linked subunits (α and β) and have small C-terminal cytoplasmic domain and large N-terminal extracellular domain. Both α and β subunits have several homologies (α:18 and β:8), and up to now 24 combinations have been reported. Integrins (β subunits) are physically connected to actin filmament with various linker proteins, such as talin, a-actinin and vinculin. Each unique integrin shows the specificity for the extracellular ligands and distinct functions in cell. Most integrins recognize tripeptide arg-gly-asp (RGD) sequence in many extracellular proteins [5]. RGD sequence serves as a shared binding site while the specificity is generated by a second binding site specific for each protein.

Besides the mechanical linkage, integrins have a significant function in signal initiation and modulation, which is characterized by the bidirectional signaling pathway between ECM and CK [6, 7]. The ligation of integrins with their ECM proteins induces intracellular biological processes (Outside-In signaling), such as cytoskeleton formation, phosphorylation of proteins and gene expression. The intracellular signals regulate the affinity of integrin-protein bindings by modulating conformational changes of integrins and the clustering of integrins (Inside-out signaling) [8]. The mutual collaboration with other signaling proteins is the special feature of integrins. Integrins affect the expression and activity of other integrins and other types of adhesion molecules by cross-talking. The cooperation with receptor tyrosine kinases (RTKs) amplifies signals and enhances the efficiency of the regulation of various biological processes. Integrin-ECM interaction activates growth factor receptors and expedites binding with ligands [9]. For example, the collaboration of erbB2 and α6β4 enhances the activity of phosphatidylinositol 3-kinase (PI3K), which promotes motility and invasiveness of carcinoma cells [10]. Some integrins can directly regulate growth factors. The co-clustering of integrins and growth factor receptors induces ligand-independent signaling of growth factor receptors [11].

1.3 Cell spreading determined by integrin binding and actin filament dynamics

Cells continuously regulate their shape in order to adapt themselves to the environment and to fulfill their task by modulating the dynamic structure of cytoskeleton (including acin filament, intermediate filament and microtubule). Cell spreading is a cytoskeletal construction process for membrane extension on the ECM surface, leading to fried-egg shaped morphology. As cells spread on the ECM substrate, they show characteristic morphology. The stress fibers cross the cell body, connecting focal adhesions which anchor the cell body to the ECM protein substrate. In the periphery of the cell body the thin sheet-like lamellipodia and spike-like filopodia are frequently observed. These structures are continuously reorganized for maintaining the cell shape and for coping with the external stimuli.

The anchorage site of well spread cells to the substrate can be divided into two structures, focal adhesion (FA) and focal contact (FC). FA is densely integrated with integrin bindings and connected with actin stress fiber. The stress fibers generate contractile force between two FA (The mechanical stress is inevitable for maintaining FA). The periphery of the cell body, where FCs are frequently observed, has more dynamic in actin filament formation, especially in the leading edge of lamellipodia. The characteristic lamellipodia (actin filament meshwork) and filopodia (actin filament bundle) are constructed by polymerizing actin monomers based on the FC. FC can be transformed into FA or disappear. The actin polymerization is critically influenced by specific integrin binding and subsequent signaling. The ligation of integrin activates small GTPases Rho family [12] leading to the sequential activation of WASP family and then Arp2/3 complex, which regulates overall actin dynamics for lamellipodial and filopdial protrusions [13, 14].

The initiation of a cascade of events regulating the cell spreading is the integrin binding with ECM proteins. Indeed, experimentally it was demonstrated that the rate and extent of spreading is mediated by integrin binding and affected by the density of ECM ligands [15, 16]. Also, ECM condition affects the cell spreading patterns [17].

1.4 The phenotype of oncogene expressing cells

Tumor cells are often characterized by being less adherent, more motile and more compliant than normal cells. In order to accomplish the metastasis, tumor cells have to break their connections (intercadherin interactions) to neighboring cells and loosen the adhesion (integrin bindings) on the basement membrane and then, digest, penetrate the basal lamina, and migrate to reach the blood vessel for gaining the access the circulatory system. These phenotypic behaviors are closely related to the fact that tumor cells exhibit the different signaling mechanism initiated by oncogenes. The abnormal activation of oncogenes affects gene expression and alters the integrin levels on cell surface and actin cytoskeleton network structures. Levels of integrins of oncogene expressing cells differ according to the cell type and the transformation system. For example, RSV-transformation of rodent fibroblast line (rat1) down-regulates α5β1 integrin, while ErbB-2, which is a dominant oncogene in breast cancer, up-regulates α5β1 integrin. Thus, each oncogene induces characteristic changes of phenotype in certain environment. Since each integrin has specific function and affinity to the counterpart ECM protein or other cell membrane proteins, differentiated level of integrins determines metastatic behavior of tumor cells. The site-specific metastasis is a good example of targeting the particular organs of tumor cells by means of over expressed integrins. Besides the role in angiogenesis, αvβ1 integrin promotes the attachment on the blood vessel wall, which is critical to be arrested under hydrodynamic flow conditions. Overexpression of α6β4, a laminin receptor, relates with migratory capability of epithelial and carcinoma cells[18]. Also, α6β4 integrin cooperates with ErbB2 in the mammary epithelial tumorigenic process [19]. Therefore, the evaluation of the integrin-mediated adhesion on specific ECM proteins provides us useful information of tumorigenic and metastatic phenotype. The comparison analysis of oncogene expressing cells with normal cells in terms of cell adhesion is helpful for

identifying the effect of the specific oncogene on the expression of integrins and for obtaining direct evidence of cellular behaviors, such as spreading, proliferation and survival.

The integrin-mediated cell adhesion can be modified by various methods. Simply the cell adhesivity can be reduced by blocking the integrin bindings with ECM proteins using soluble peptides containing an RGD sequence. The affinity of integrin for soluble ligands is less than insoluble ECM proteins and the blocking effect does not persist. Also, the integrin binding with soluble ligand may initiate uncontrolled signaling mechanism. The variation of cellular adhesivity can be obtained by treating the cell with tumor promoter. 12-O-tetradecanoylphorbol-13-acetate (TPA) triggers a series of events leading to the alteration of cellular shape and the loss of cell adhesivity. TPA activates membrane bound protein kinases C (PKC), and PKC depolymerizes the actin filaments. However, since it affects various cellular mechanisms, TPA may not be ideal for cell adhesion study. In contrast, using oncogene expressing cells for adhesion study has several advantages. The established cell line by the transfection of active oncogene maintains consistent and stable phenotype in terms of morphology and expressed integrin levels. The specific integrin or structural components can be manipulated by gene silencing techniques such as siRNA knock-down.

The receptor tyrosine kinase ErbB-2 (also known as HER2/neu, NeuT is a rat analogue of ErbB-2) plays important roles in signal transduction leading to the pathogenesis of breast cancer [20]. The ErbB-2 gene is amplified and ErbB-2 is over-expressed in 25~30% of breast cancers and has been a major target of breast cancer diagnosis and treatment [21]. The high level of ErbB-2 is associated with increased disease recurrence and worse prognosis [22]. ErbB-2 has been reported to be closely related to the expression of integrin receptors. The retroviral transfection of normal cells with pBabe-NeuT induces the genetic modification of integrin genes and up-regulates α5 integrins. The activation of ErbB-2 led to selective up-regulations of α integrin subunits, such as α2, α3, α5 and αV, and the up-regulated α5β1 integrin enhanced long-term cell adhesion on FN [23].

1.5 The measurement of intrinsic adhesivity and cell spreading process

For the quantitative evaluation of cell-surface interactions, the assessment of cell adhesion strength, which indicates the resistance to the applied shear stress on cell body, has been widely attempted with various methods. In the parallel plate flow assay, a homogenous flow on the cell surface induces shear stress which is proportional to the flow [24]. Thus, this assay provides controlled and reliable shear stress, which can not be achieved by the simple rinsing assay. Centrifugation and spinning disk adhesion assays use the centrifugal force and the shear stress generated by the rotation, respectively [25, 26]. Whereas, in the centrifugation device, the cell sample is spun with the rotor in the media, the spinning disk generates shear flow over the cell layer. Both assays are reported to provide quite quantitative and controllable operations. However, these techniques have limitations in providing a direct measure of the intrinsic adhesivity of the cell-surface interaction, especially if used to monitor adhesion beyond the initial attachment phase. The resistance of cells to detachment by flow depends not only on the number, distribution and strength of the adhesion bonds formed, but also the spread area and the surface topography of the cells. As cells spread, resultant drag and torque on the cell due to flow are dramatically decreased, while the increasing contact area enhances the ability to resist detachment.

Recently, several attempts have been made in order to quantify the cell spreading and to determine the effects of property of substrate (e.g. ligand density) on the rate of cell spreading. Dubin-Thaler et al. monitored the cell spreading and quantified the rate of spreading in nano-scale and tried to describe the cell spreading with two distinct spreading modes [17]. Reinhart-King et al. investigated the changes in cell shape and traction force on polyacrylamide gels, of which ligand densities were differently manipulated and reported that the rate and extent of spreading increase with the density of ligands on the substrate [16]. Roberts et al.

demonstrated a functionalized surface with self-assembled monolayers (SAMs) presenting RGD for cell-surface interactions [27].

1.6 Thickness Shear Mode resonator

A TSM sensor is capable of detecting nano-scale changes in mass and in mechanical properties of interfacial materials on the sensor surface [28]. A TSM sensor, which uses the piezoelectric effect (The applied voltage generates the mechanical stress and displacement, vice versa), generates characteristic shear waves penetrating into a contacting media according to oscillating voltage frequencies (Fig. 1.1A). The vibration of the TSM sensor is affected by the mass and mechanical properties, such as density and viscosity, of the interfacing material within the probing depth (Fig. 1.1B). The resonant frequency shift and the scattering parameter (S21) change have been widely used in describing the behavior of the vibration. Since the cell adhesion process changes these mechanical properties of the interface between cells and TSM sensor surface, the analysis of these measurands provides us the information about the cell-surface interaction during the cell adhesion process. In this study, S21 of 3rd harmonic frequency (15 MHz) has been measured with a network analyzer (S21 is measured by sending a signal into the sensor device and detecting what returns as a reflex.) and converted into the resistance change (ΔR) of the equivalent circuit (See appendix 1). Thus, ΔR indicates the energy dissipation due to the change of mechanical properties during the cell adhesion process. This parameter contains distinct features from resonance frequency shifts for analyzing the cell adhesion process used by others [29-31].

1.7 Objectives

Cell adhesion is a dynamic process mediated by continuous and complex molecular interactions with an extracellular matrix (ECM). The identification of cell-substrate interactions and their kinetics is important in understanding the cellular behaviors, such as

morphologic change, growth, migration and differentiation of cells. However, the quantitative and real-time assessment has been limited. Previous studies of cell spreading have focused on morphological changes assessed by microscopic observations and the image processing. This type of analysis does not provide direct assessment of adhesivity or mechanical properties of the cell. Also, a number of techniques for quantifying cell adhesion strength have been developed to more directly assess adhesivity; however these techniques do not provide real time analysis of cell-substrate interactions during the spreading process. TSM sensor measurement is able to provide the quantitative information about the cell-substrate interaction and its real time progression. More importantly, the functional state of cell adhesion molecules (CAMs) affected by various factors, such as amount of CAMs, their activation, and governing signaling mechanism can be assessed.

The main focus of this study was to establish a new experimental and analytical foundation for assessing cell-substrate interactions and cell adhesion process using TSM sensor. The specific effects of receptor-mediated adhesion, the glycocalyx, and surface charge on initial attachment and long term adhesion of cells were investigated. Intrinsic properties and cell spreading kinetics were assessed by assigning the physical meaning to the characteristics of sensor response to the cell adhesion process.

Aim 1; Characterize cell-surface interactions in terms of TSM sensor response to the cell adhesion process.

Hypothesis 1: Interactions of integrin, glycocalyx, and surface charge of cells with the substrate contribute to different aspect of cell adhesion. These interactions are reflected to the sensor responses.

Aim 2; Characterize the cellular specific interaction and spreading kinetics and describe the functional phenotype of oncogene expressing cells.

Hypothesis 2: Intrinsic adhesivity and cell spread area change is related to the initial increasing slope and change of ΔR, respectively. The sensor response distinguishes the adhesion of oncogene expressing cells from normal cells.

Aim 3; Evaluate the stiffness and deformability and characterize their effect on the initial attachment.

Hypothesis 3: The alteration of cytoskeleton dynamics induced by the oncogene signaling changes mechanical properties of cells. Cell stiffness and deformability is related to the initial change of ΔR.

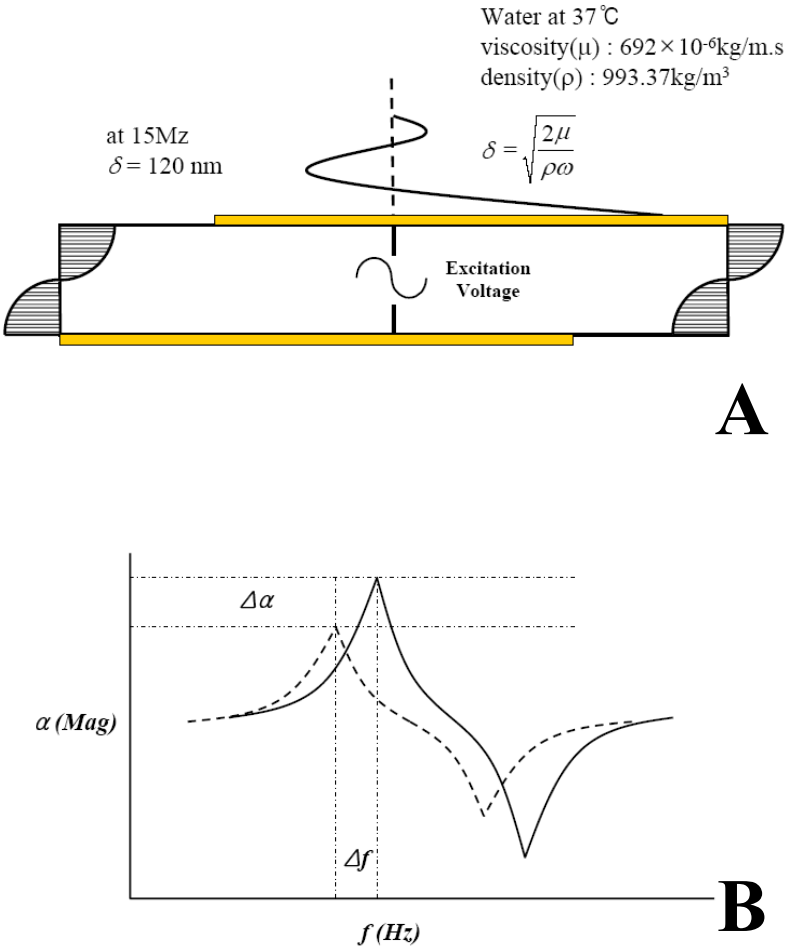

Figure 1.1 The mechanism of the operation of TSM sensor and TSM sensor responses in network analyzer (B). By the piezoelectric effect, TSM sensor laterally vibrates according to the applied voltage and this vibration is affected by the mechanical properties, such as density and viscosity, of the interface that is very close to the sensor surface. Thus, the cell adhesion process, accompanying mechanical property changes, can be reported by the sensor readings.

CHAPTER 2

CELL-SURFACE ADHESIVE INTERACTIONS

2.1 Introduction

Cell adhesion is a complex process involving physical interactions, chemical binding events, and biological signaling processes. Cellular adhesion plays important roles in the regulation of cell behavior, such as the control of growth, differentiation during development and the modulation of cell migration in wound healing, metastasis, and angiogenesis. Cell adhesion has been one of the important criteria for evaluating the tissue integration of implanted biomaterials. In particular, quantitative characterization of cell adhesion and its kinetics provides valuable information for the development of biomaterials. Therefore, a lot of effort has been made to elucidate dynamic mechanism of cell adhesion. Current techniques for evaluating the cell spreading and cell adhesion strength are labor intensive and destructive (e.g. flow detachment assay). Especially, they are not sufficient in providing the detailed kinetics of adhesion process. Initial attachment and spreading patterns have been studied and various techniques have been introduced to quantify the cell adhesion strength [17, 26, 32-34]. Morphology and topographical distribution of focal adhesions have been investigated in real-time with confocal microscopy and immuno-staining technique [35, 36].

Recently, the Thickness Shear Mode (TSM) sensor technique has been used to detect cells adhering to the sensor surface. Since TSM sensor is capable of detecting nano-scale changes in mass and mechanical properties of interfacial material, it is possible to detect ligand-receptor binding in real time. This technique has been used in monitoring the cell adhesion process using resonance frequency shifts [29, 30]. Wegener et al. [37] have shown that different cell types have their own characteristic frequency changes when they formed confluent monolayers, and tried to explain frequency shifts with geometrical properties of

cells. Janshoff et al. [31] assumed that a monolayer of cells had visocoelastic properties and tried to estimate viscosity of cell monolayer by comparing impedance measurements with an electromechanical model. Marx et al. [38] has shown that morphological changes of cells due to the depolymerization of cytoskeleton caused frequency and resistance shifts. Li et al. [39] assessed the integrin-mediated cellular interactions with ECM proteins by evaluating the bandwidth shift.

In this study, our goal was to correlate sensor readings (specifically, the motional resistance) with adhesion strength. Furthermore, we studied the contributions of the various molecular components of the interface to the kinetics of cell adhesion. Experiments were conducted to assess the cell adhesion processes that were affected by inhibition of integrin binding, degradation of heparan sulfate proteoglycan (HSPG) and surface charge modification. The real time sensor measurements were characterized and interpreted in terms of distinct phases of the cell adhesion process.

2.2 Material and methods

2.2.1 Endothelial cell culture.

Bovine Aortic Endothelial Cells (BAECs) were isolated from calf ascending aorta as previously described [40]. The BAECs were cultured in complete media [Dulbecco's modified Eagle's medium (Mediatech, Inc., Herndon, VA), 100 units/ml penicillin, 100 μg/ml streptomycin, 250 ng/ml amphotericin B (Sigma Chemical Co., St. Louis, MO), 2 mM/ml L-glutamine and 10% heat-inactivated calf serum (Invitrogen Co., Carlsbad, CA)] in a humidified, 37ºC incubator with 5% CO2 in air. Passage numbers were between 6 and 14. Cell suspensions were made by treating the confluent monolayer of BAECs with 0.25% trypsin for 90 sec, centrifuging at 200 g for 5 min, and resuspending in serum-free media [Dulbecco's modified Eagle's medium (Mediatech, Inc.), 100 units/ml penicillin, 100 μg/ml

streptomycin, 250 ng/ml amphotericin B (Sigma Chemical Co.), 2 mM/ml L-glutamine (Invitrogen Co.)].

2.2.2 TSM sensor device and measurement system.

The sensing device was built on a disk-shaped AT-cut quartz crystal (f_0 = 5 MHz) by attaching a Teflon cylinder of which inner diameter and height were 11 mm and 8 mm respectively. The 0.33 mm thick crystal was 14 mm in diameter with gold electrodes 7 mm in diameter. The sensor device was then placed in a humidified, 37ºC incubator with 5% CO_2 in air. The sensor device was connected to a network analyzer (HP 4395A), and a personal computer was used for controlling the network analyzer and collecting the data. At the fundamental frequency (5MHz), sensor readings contained fluctuations likely due to insufficient energy trappings as described by others [39]. Thus, the results reported here are for the sensor operating at 15 MHz frequency. The TSM sensor response was measured using Network Analyzer (NA). With our system, tracking the frequency change gave a noisy signal (see Fig 2.1A and B insets), while the resistance changes at resonant frequency were very stable and robust. Thus, we used the changes in resistance (ΔR) caused by the biological events at the interface between cells and TSM sensor surface. Resistance changes (ΔR) were acquired every 30 seconds.

2.2.3 Surface coating of TSM sensor.

All experiments were performed in serum-free medium to avoid variability due to uncontrolled concentration of adhesion molecules and growth factors present in serum. Except as noted, a gelatin coating of the sensor surface was used as the adhesive substrate. Gelatin coating was used to provide a uniform surface presenting Arg-Gly-Asp (RGD) peptide sequence for integrin binding. The TSM sensor was immersed in 0.5% (v/v) gelatin solution (Sigma Chemical Co.) for 30 min at room temperature. The surplus of gelatin was removed by aspiration and the surface was rinsed with PBS two times. The thickness of the gelatin coating was ~10 nm, as assessed by AFM, and produced a negligible change in sensor readings. To

create a net positive charge on TSM sensor without gelatin, it was coated with poly-D-lysine (PDL, mol wt 30,000-70,000) solution (0.1mg/ml in PBS) for 20min. It was rinsed with PBS twice and allowed to dry overnight.

2.2.4 Soluble Arg-Gly-Asp (RGD) treatment.

The RGD sequence in the extracellular matrix (ECM) is a primary ligand for integrin receptors. To block integrin binding to gelatin-coated sensor surface, cell suspensions were treated with soluble RGD peptide (2 mM, Sigma Chemical Co.) for 10 min at room temperature [37].

2.2.5 Heparinase III treatment.

Heparinase III is an enzyme that digests heparan sulfates selectively from the membrane surface. The monolayer of BAECs was incubated in Heparinase III (30 mU/ml) in phenol red free Minimal Essential Media (MEM) [Sigma Chemical Co., 100 units/ml penicillin, 100 μg/ml streptomycin, 2 mM/ml L-glutamine, and 1% BSA (Sigma Chemical Co.)] for 3 hrs [41]. After the incubation, the monolayer was rinsed with MEM twice. The cell suspension was made with same procedure as described above and then was put into the sensor device.

2.2.6 Experimental Protocol.

Prior to adding the cell suspension, 0.1 ml of serum-free media was placed in the TSM sensor chamber and allowed to equilibrate to 37ºC. The equilibrium of the temperature was confirmed by checking the stability of sensor signal. Next, 0.4 ml of cell suspension (37ºC, 3.75×10^5 cells/ml) was gently pipetted into the chamber for a final concentration of 3×10^5 cells/ml. The total number of cells per sensor area was approximately the density of a confluent monolayer of ECs. The initial projected area of the unspread cells was approximately 15~20% of the sensor surface area. The density of cells was chosen to give the maximal response without overly constraining their ability to spread.

2.2.7 Optical measurement.

Ten sensor chambers were prepared. Five of them were coated with gelatin as described above and the rest were used without any treatment as bare surface. Cell suspensions (3×105 cells/ml) of 0.5 ml were placed in each sensor chamber and incubated (37ºC, 5% CO2). At each time point (10 min, 20 min, 30 min, 40 min and 50 min), following inoculation, one of the sensors was rinsed to remove the weakly attached and unattached cells from the surface. Care was taken to make the rinsing procedure consistent between trials. After removing the cylinder from the sensor, the sensor was held at approximately 45˚ angle (from horizontal) while 2ml of PBS was slowly pipetted onto the upper edge of the sensor and allowed to flow down the tilted surface driven by gravity alone. Cells that remained attached after two rinses were stained with Calcein Green (Invitrogen Co.) to allow visualization on the opaque sensors. Calcein Green is introduced to the cells in a non-polar ester form that can diffuse across the plasma membrane. It is then modified by nonspecific esterases into a polar fluorescent molecule that cannot escape the cell if the membrane is intact. Thus, it also serves as a viability marker. The cells were imaged using an epifluorescence microscopy, and the total number of cells in 5 randomly selected microscope fields was counted.

2.3 Results

2.3.1 Characterization of TSM sensor readings.

The time course of the resistance change (ΔR) following inoculation was used to characterize the cell adhesion process (Fig. 1). In the typical response, following an initial delay time (~10 min), there was a sharp increase in resistance to a new plateau (primary plateau). Subsequently, there was slower increase in resistance to a new minimum value (secondary plateau) that either persisted or gradually increased or decreased. The predicted sedimentation time was approximately 10 min. The changes in adhesion response due to the various interventions were characterized by changes in the delay time, the slope of the initial decrease in ΔR, and the size of ΔR at the primary plateau.

2.3.2 Correlation of TSM sensor readings with optical cell adhesion measurement.

In parallel experiments, cell suspensions were placed on multiple TSM sensors. For one, ΔR was recorded continuously for 2 hrs. For the others, the experiments were stopped at various time points after inoculation to evaluate adhesion strength. The TSM sensor surface was rinsed twice with PBS removing unattached or weakly attached cells.

A detailed comparison of time courses of ΔR shows that the cell adhesion on the bare sensor surface had a longer delay time before there was any detectable ΔR than that on the gelatin coated sensor surface (25 vs. 10 min). Furthermore, the slope of the initial increase in ΔR and the size of ΔR at the primary plateau were both smaller than those on gelatin coated sensor by a factor of 5 (Fig. 2.2A).

The results for cell adhesion on the two surfaces showed a similar pattern as the sensor readings (Fig. 2.2B). The comparison of time course and degree of cell adhesion between the bare and gelatin-coated surfaces was consistent with that of sensor readings. The cell adhesion was detected much greater on the gelatin-coated sensor surface compared to the bare surface. Similarly, the maximum rate of change in the number of adhered cells and the final number of adhered cells (at 50 min) were much greater on the gelatin coated sensor (Fig. 2.2B). The change in the number of adhered cells with time corresponded with the change in sensor readings (Fig. 2.2C). However, the relationship was slightly different for cells on bare sensor compared to the gelatin-coated surface. It was noted that there were also differences in the morphology of the cells that were attached. While cells on bare sensor surface remained round in shape, cells on gelatin coated surface were well spread (Fig. 2.3).

2.3.3 Integrin binding inhibition with soluble RGD.

Soluble RGD peptides were used for blocking the integrin binding with ECM molecules. The delay time was similar from both RGD treated and untreated controls. However, pretreatment with soluble RGD significantly retarded the rate of the initial ΔR (Fig. 2.4A). After the delay time, control cells showed the typical rapid increase to a primary

plateau, followed by an additional increase to the secondary plateau (Fig. 2.4B). In contrast, integrin blocking caused a slower increase to the secondary plateau with no primary plateau. There was no difference in the secondary plateau and long term ΔR. Fluorescent images of adherent cells were consistent with the TSM sensor measurement (Fig.2.5). The control showed more adherent cells at 1 hr than with RGD treatment, while both showed similar cell numbers at 20 hrs.

2.3.4 TSM sensor coating with PDL.

To evaluate the influence of surface charges on cell adhesion, we coated the sensor surface with the positively charged PDL. The PDL coating caused a reduced delay time compared to the control; however, the rate of change in ΔR was similar for both adhesions. Cells on gelatin layer showed the typical time course of cell adhesion (Fig. 2.6A). Despite the apparent facilitation of initial adhesion by PDL, the primary plateau ΔR was not as great as with gelatin, and at longer times the signal returned to baseline values (Fig. 2.6B). Visual inspection at 20 hrs showed that the cells had become detached (data not shown).

2.3.5 Degradation of HSPGs with heparinase III.

To evaluate the role of the glycocalyx in the adhesion process, we pretreated cells in culture with Heparinase III. It has been shown that this treatment removes a significant portion of HSPG from the cell surface [41, 42]. Heparinase III treatment had no effect on the delay time or the kinetics of the initial increase in ΔR. However, digestion of the HSPG significantly reduced the steady state ΔR, and this difference persisted for the duration of the experiment (Fig. 2.7).

2.4 Discussion

We verified the correlation between cell adhesion strength and ΔR reported by the TSM sensor. Cell adhesion strength was estimated with simple rinsing assay. While this technique is not quantitative in terms of the detachment forces, care was taken to ensure consistency

from trial to trial. There are existing techniques for assessing cell adhesion strength through the application of more controlled and quantifiable shear flows [26, 32, 34]. However, these techniques do not provide a direct measure of the intrinsic adhesivity of the cell-surface interaction, especially if used to monitor adhesion beyond the initial attachment phase. The resistance of cells to detachment by flow depends not only on the number, distribution and strength of the adhesion bonds formed, but also the spread area and the surface topography of the cells. As cells spread, resultant drag and torque on the cell due to flow are dramatically decreased, while the increasing contact area enhances the ability to resist detachment (independent of number and strength of adhesion bonds per se) [32]. As the adhesion process progresses, there is likely to be a distribution of morphologies at a given time point.

The TSM sensor technique interrogates directly the cell-surface interface and therefore provides different information than the flow detachment assay. Flow detachment assays provide information about the threshold for detachment (with the caveats on interpretation listed above), but the sensor readings reflect the contributions of both weakly and strongly attached cells. While the kinetics of the changes in sensor readings closely match the changes in adhesion, the changes in ΔR do not scale linearly with the changes in apparent adhesion strength when comparing adhesion under different conditions. For example, in the initial phase of adhesion when most of the cells are still only weakly attached, the sensor appears to have greater sensitivity than the adhesion assay indicated by the higher slope in ΔR v. number of adherent cells at the early time points (lower left corner of plot in Fig. 2.2C). This suggests that cells below the detachment strength threshold of the rinsing experiment also contribute to the ΔR signal. During the spreading process, the strong synergy between increased contact area and reduced height profile of the cells makes them much more resistant to detachment independent of the nature of the cell-substrate interaction. Further evidence that the TSM sensor readings reflect changes in the cell-surface interface rather than adhesion strength, per se, comes from a comparison of the adhesion on the bare sensor surface and the

gelatin-coated surface (Fig. 2.2C). The number of attached cells at 50 min on the bare sensor was similar to the number attached at 20 min, on gelatin (Fig. 2.2B); however, in the acoustic measurement, cell adhesion on gelatin surface gave a 3 fold greater ΔR than on the bare surface (Fig. 2.2A). The majority of the cells on bare surface were rather spherical shape, while the cells on gelatin were well spread. Differences in relative area of close contact between the cell membrane and surface [29] and changes in mechanical properties due to the developing cytoskeleton [43] may both contribute to the sensor readings

The kinetics of cell adhesion depend on the physical, chemical and biological interactions between the cell and ECM molecules. While the slope and size of the ΔR signal correlates to the kinetics and strength of the initial adhesion to the substrate, the delay time suggests an energy barrier to the formation of the initial adhesive contact. Assuming a constant sedimentation velocity (i.e. neglecting cell-cell interactions), the number of cells on the surface increases linearly with time from the initial inoculation. The sedimentation process was completed by approximately 10 min. However, the TSM sensor readings did not detect the presence of the cells on the sensor surface during this period. In a study of the passive adsorption of lipid vesicles, which may be considered a model cell membrane without binding molecules or a glycocalyx. Reimhult et al. [44] reported no delay between the delivery of vesicles to the sensor surface and the change in sensor readings. Bell et al. [45] developed theoretically the idea that nonspecific repulsive forces compete with the specific attraction between cell surface receptors and their extracellular matrix ligands. Our data support this idea, and the TSM sensor technique presented here could be used to generate quantitative estimates of the energy barrier.

The initial attachment of cells on the PDL coated TSM sensor further supports the energy barrier concept. Since the cell membrane is covered with negatively charged glycocalyx, the electrostatic attraction between cell membrane and positively-charged PDL surface would tend to lower the energy barrier for cell adhesion. The reduced delay time for

adhesion on PDL is consistent with this interpretation. Furthermore, the finding that electrostatic attraction can facilitate cell-surface interaction is consistent with previous experimental results [46, 47]. The failure of long-term cell adhesion on PDL in serum-free media, indicated by the return of ΔR towards the baseline, was due to the absence of ECM molecules. While in complete media, proteins such as fibronectin and vitronectin are absorbed onto the surface, the PDL substrate in serum-free media does not provide ECM molecules. PDL alone does not support integrin binding and focal adhesion formation.

Once adhesion is initiated, the kinetics of the rapid increase in adhesion strength appears to be mediated by integrin binding between cellular membrane and the substrate. Using soluble RGD to occupy integrin receptors showed an effect on the initial adhesion process while degradation of HSPG had no effect on the initial kinetics. This finding is consistent with known properties of integrins and HSPG. Integrins produce high affinity, specific binding to ECM ligands while HSPG acts as a low affinity co-receptor that stabilize and strengthen the integrin binding, facilitating the focal adhesion formation [48, 49]. The result that heparinase III treatment reduced steady state adhesion strength supports this role for HSPG. HSPG is also known to regulate the cell signaling mechanisms triggered by binding to soluble and insoluble extracellular ligands (e.g. growth factor) [50]. However, because our experiments were performed in serum-free media, this role for HSPG in the adhesion process was minimized.The long term adhesion in the presence of soluble RGD was not different from controls. Several explanations for this behavior are possible. First, steady state adhesion in a spread cell may require fewer integrin bonds than the initial attachment and spreading process. Second, once the cell is spread on the surface, the integrins and their ECM ligands are in close apposition while the reaction with soluble RGD will still be transport limited. Third, soluble RGD may be bound and internalized by the cell, lowering concentration with time. All the experiments described in this work were performed in the absence of serum. Serum contains a variety of adhesion molecules and growth factors. The composition of these components

present in any given lot of serum is variable. The adsorption of adhesion molecules onto surfaces is rapid and would, thus, contribute an undefined adhesivity to the sensor surface and confound our attempts to control and vary surface properties. To evaluate the possible effects of removing serum, we performed several experiments with serum (data not shown). For adhesion on gelatin coated sensors, the presence of serum caused a small increase in the magnitude change. On the bare sensor, serum significantly enhanced the adhesion response. The presence of adhesion molecules and growth factors appeared to have a synergistic effect since pre-coating the sensor with serum containing medium produced only a small increase in adhesion when the cell were seeded in serum-free medium.

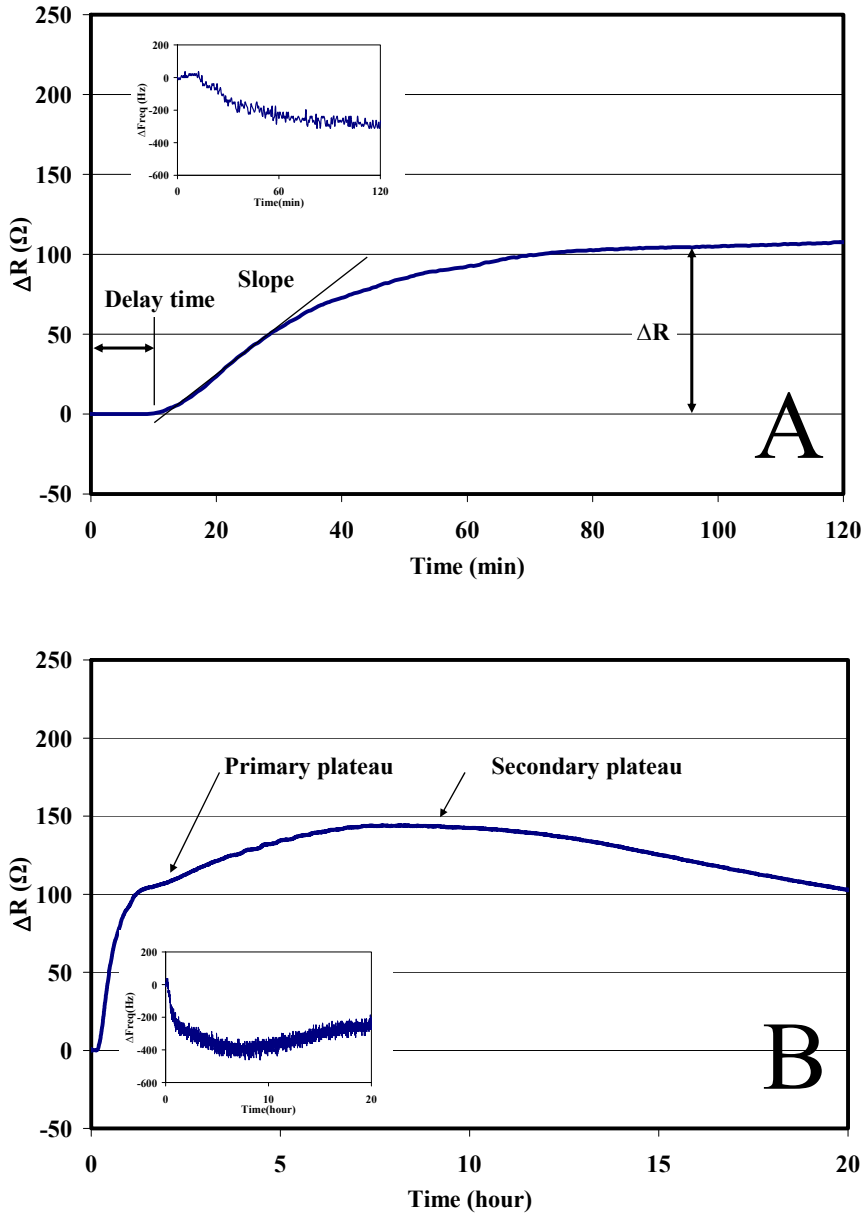

Figure 2.1 Time course of △R due to the adhesion process of endothelial cells for the initial adhesion (A) and the steady state adhesion (B). Cell adhesion process can be characterized by changes in the delay time, the slope of the initial decrease, and the size of □R at plateaus.

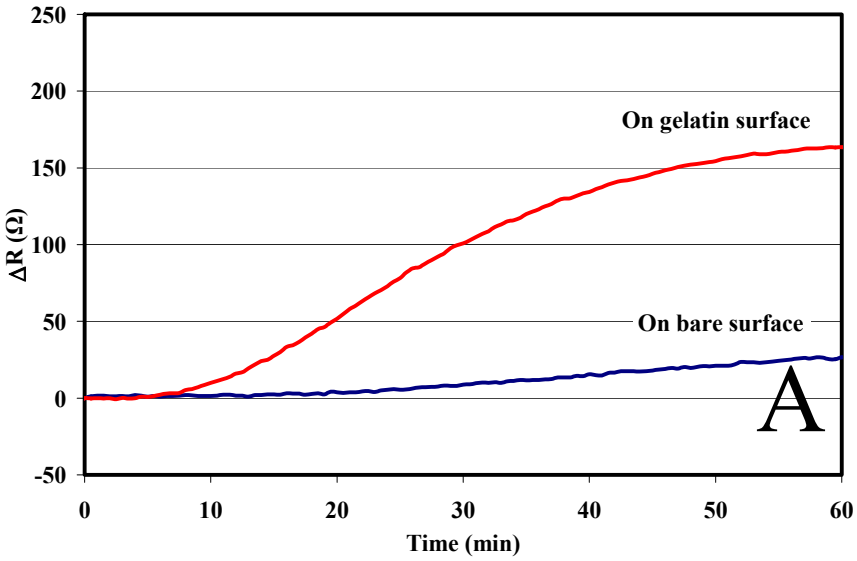
250
200
150
100
50
0
-50
ΔR (Ω)
On gelatin surface
On bare surface
A
0
10
20
30
40
50
60
Time (min)

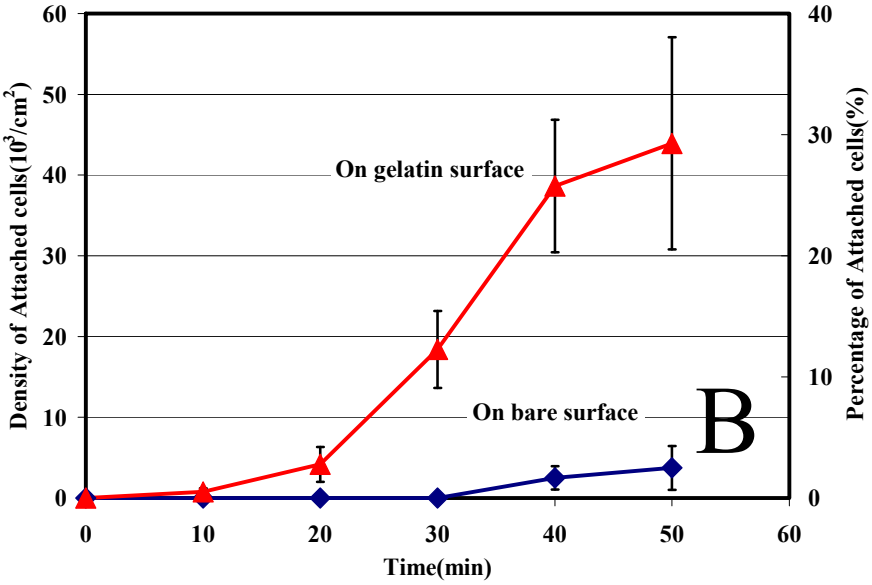
60
50
40
30
20
10
0
Density of Attached cells(10³/cm²)
40
30
20
10
0
Percentage of Attached cells(%)
On gelatin surface
On bare surface
B
0
10
20
30
40
50
60
Time(min)

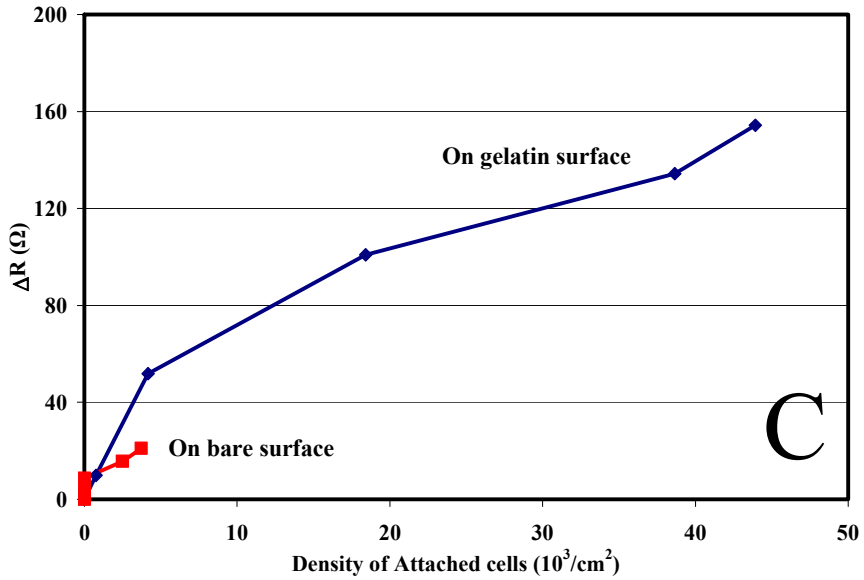

Figure 2.2 Correlation of sensor readings with optical observation. The cell suspensions in serum-free media were placed on bare and gelatin coated TSM sensors in the incubator (37ºC, 5% CO2). The area of sensor surface and the number of cells were 0.95 cm2 and 150×103. The sensor readings (▵R) were recorded for 1 hrs (A). For the optical observation, TSM sensors were rinsed with PBS at various time points during the incubation and adherent cells were counted with the fluorescent microscope. Optical data are presented with SD. N=5 (B). The correlations of ▵R with the number of adherent cells were shown in (C).

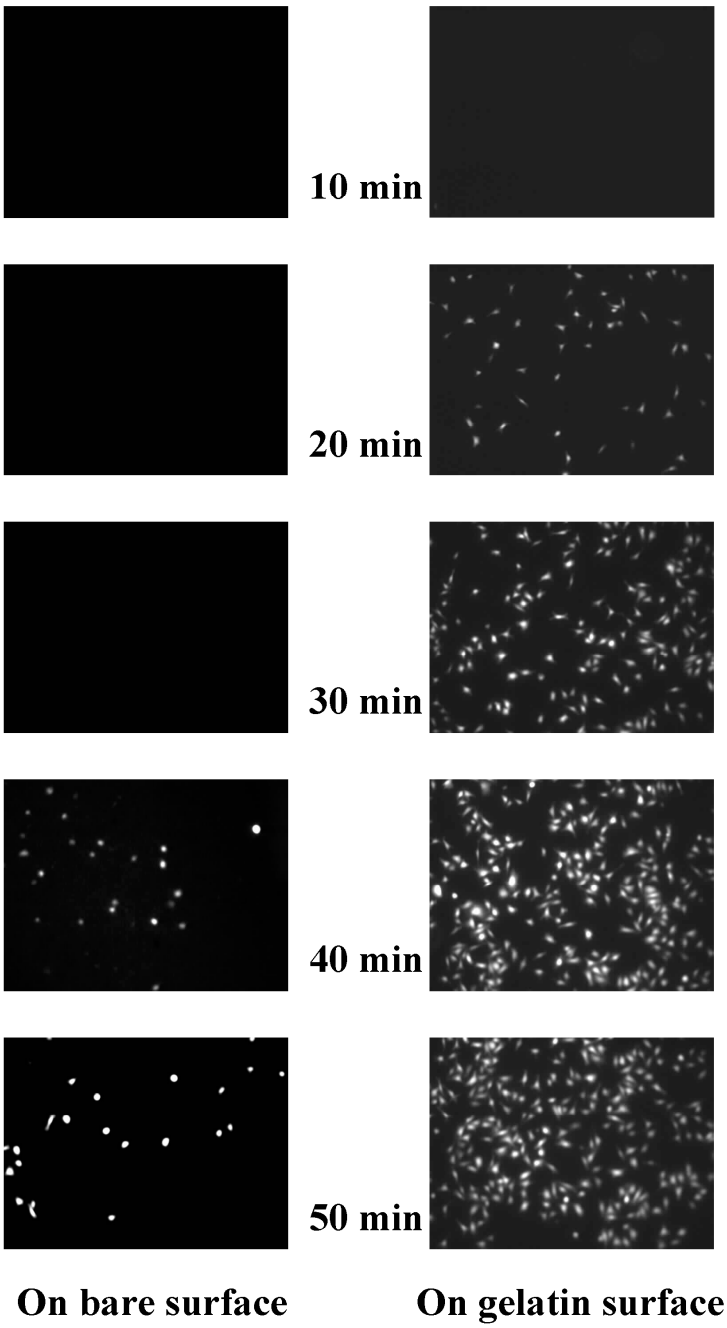

Figure 2.3 Comparison of the number and morphology of adherent cells on bare and gelatin TSM sensor after being rinsed with PBS at various time points. The adherent cells were visualized with epifluorescent microscopy. Size of each picture is 800μm×600μm

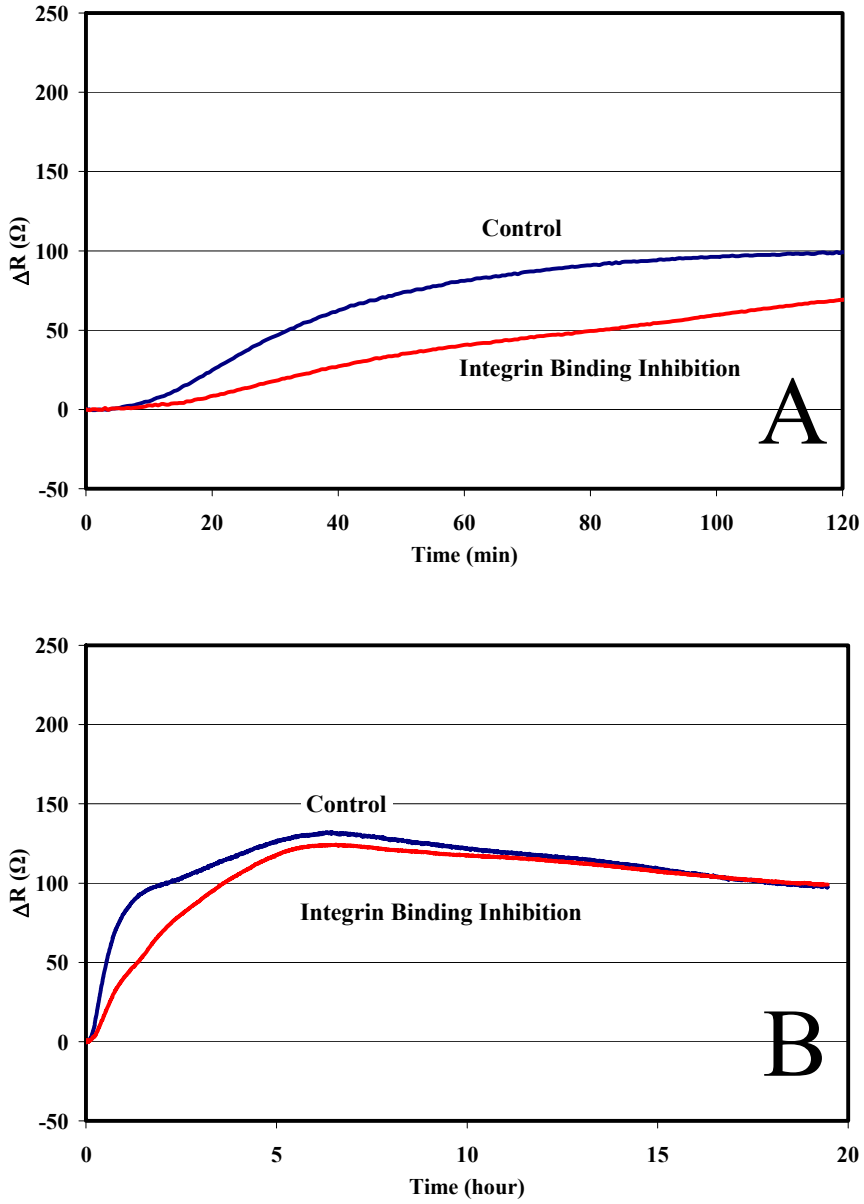

Figure 2.4 Influence of integrin binding inhibition with soluble RGD on cell adhesion process. Soluble RGD peptides (2 mM) were used for blocking integrin binding in order to inhibit the cell adhesion. RGD treated cell suspension in serum-free media was place on gelatin coated TSM sensors at the same time with control. The sensor readings (△R) of initial and steady state cell adhesion process were shown in (A) and (B) respectively.

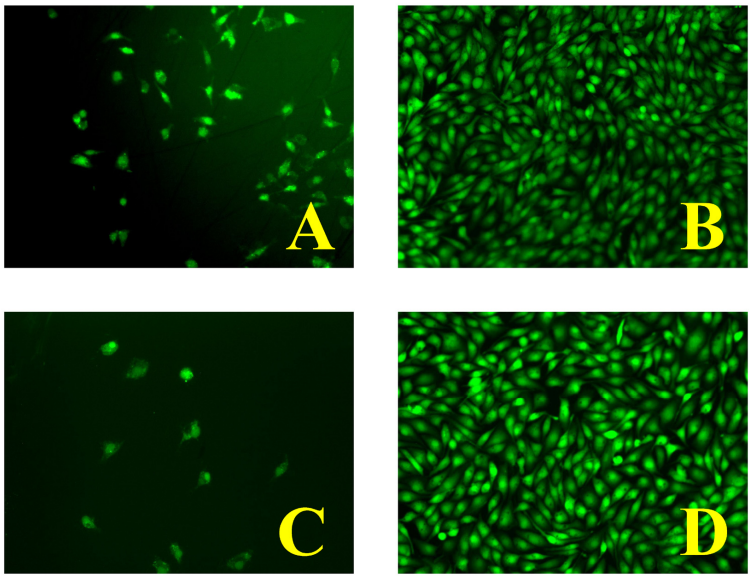

Figure 2.5 Comparison of adherent cells of RGD treated with control at 2 hrs and 20 hrs. TSM sensor surfaces were rinsed with PBS at each time point and stained: A) Control, 1 hr, B) Control, 20 hr, C) RGD treated cells, 1 hr, D) RGD treated cells, 20 hr. Size of each picture is 630 μm × 470 μm

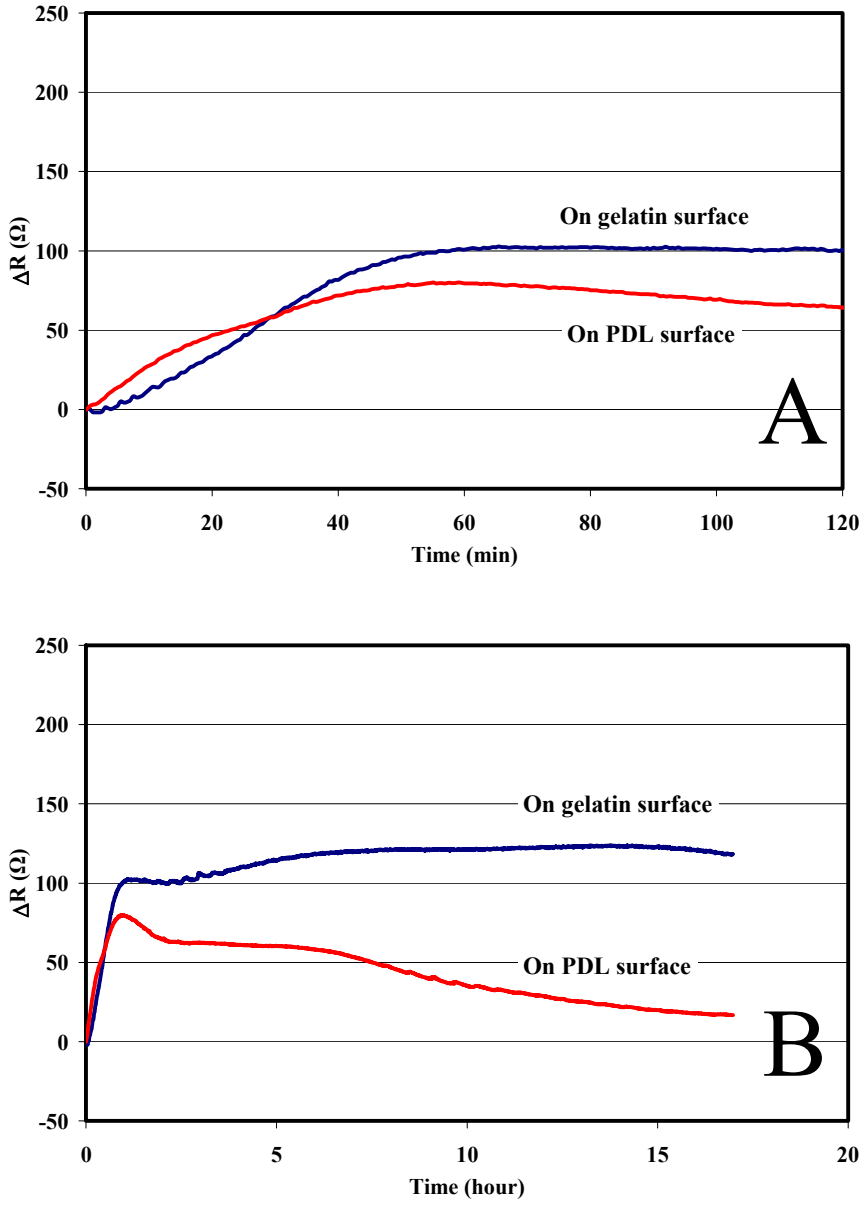

Figure 2.6 Influence of the positively charged surface on cell adhesion process. The TSM sensor surface was coated with positively charged PDL. The sensor readings (▵R) of initial and steady state cell adhesion process were shown in (A) and (B) respectively.

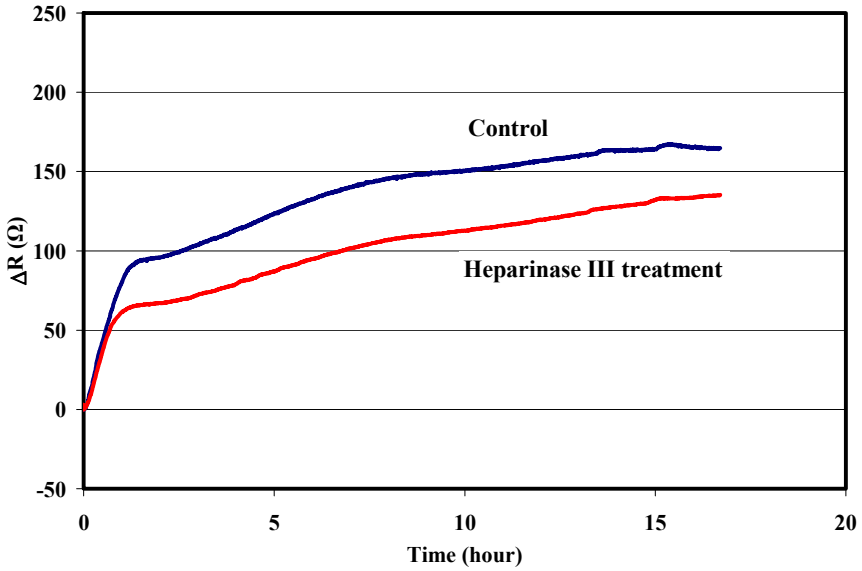

Figure 2.7 Influence of removal of HSPGs from the cell membrane on steady state cell adhesion process. The monolayer of endothelial cells was treated with Heparinase III, digesting the significant portion of HSPG from the cell surface.

Table 2.1 Evaluation of cell adhesion and its kinetics

	Sedimentation	Initial attachment & spreading	Stable adhesion
Schematic diagram of cell adhesion	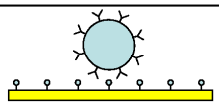	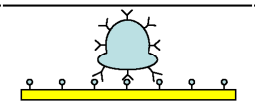	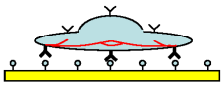
Cell adhesion interventions	Electrostatic interaction	Integrin bonds	Focal adhesion
Characterizing factors of time course of ΔR	Delay time	Primary slope & Size of ΔR at primary plateau	Size of ΔR at secondary plateau
Influenced cell adhesion kinetics	PDL layer enhanced initial interactions	Soluble RGD treatment delayed initial adhesion	Degradation of HSPGs decreased long term adhesion

CHAPTER 3

INTRINSIC ADHESIVITY AND CELL SPREADING

3.1 Introduction

Cell adhesion to extracellular matrix (ECM) proteins is critical for organization of tissues and plays an essential role in regulating cellular behaviors, such as survival, growth, differentiation and migration. During cell matrix attachment and spreading, cells undergo morphologic alterations driven by passive deformation and active reorganization of the cytoskeleton. Integrin receptors, heterodimeric transmembrane proteins, play a central role in cell adhesion and spreading. Specific integrin binding provides not only a mechanical linkage between intracellular actin cytoskeleton and ECM, but also bidirectional transmembrane signaling pathways [2, 51, 52]. Integrins recognize soluble ligands and insoluble ECM proteins and their interaction regulates cell responses such as cytoskeleton formation. Ligation of integrins with their ECM proteins activates the Rho GTPase family (including Rho, Rac and Cdc42) which is involved in cell spreading and migration [53, 54]. Rho controls stress fiber formation and the assembly of focal adhesions (FA), and Rac and Cdc42 regulate lamellipodial protrusion and filopodial extension [55].

There is abundant evidence that cell adhesivity and mechanical properties regulate cell behaviors such as migration [56, 57]. Adhesivity and deformability also control cell spreading dynamics, so an analysis of cell spreading dynamics may be useful for characterizing cell properties that contribute to the functional phenotype of cells. Changes in integrin-mediated adhesion and signaling are associated with the transformed phenotype [58, 59]. Tumor cells are characterized by changes in adhesivity to ECM, which may be related to the invasive and metastatic potential. Alterations in cell-matrix and cell-cell interactions are cell type and oncogene specific. For example, while the transfection of rodent fibroblast cells with Src and

Ras oncogenes reduces the adhesiveness to FN by impairing α5β1 integrins, the activation of oncogene ErbB2 in breast cancer up-regulates α5β1 integrin and enhances adhesion [23, 60, 61].

Previous studies of cell spreading have focused on morphological changes assessed by microscopic observations and the image processing [16, 17, 27, 62]. This type of analysis does not provide direct assessment of adhesivity or mechanical properties of the cell. A number of techniques for quantifying cell adhesion strength have been developed to more directly assess adhesivity [24-26]; however these techniques do not provide real time analysis of cell-substrate interactions during the spreading process.

We have previously used thickness shear mode (TSM) resonators to monitor cell adhesion in real-time and were able to distinguish qualitatively and semi-quantitatively adhesion kinetics of endothelial cells as a function of modifications of substrate, cell surface proteins and integrin blocking [63]. The objectives of the current study are to establish a basis for using the real time TSM resonator response to cell adhesion and spreading to describe quantitatively properties of the cell related to its functional phenotype and to demonstrate the utility of this technique to distinguish malignant epithelial cells from the normal phenotype.

3.2 Material and methods

3.2.1 Cell culture and materials

MCF-10A cells were obtained from ATCC (Manassas, Virginia) and pBabe-NeuT cDNA, encoding the rat homolog of the ErbB2, was provided by Danielle Carroll (Harvard Medical School, Boston, MA). Anti-integrin α-5 and actin (C-11) antibodies were obtained from Santa Cruz Biotechnology, c-neu antibody was obtained from Oncogene Research (Boston, MA). MCF-10A cells were cultured in DMEM/F-12 media supplemented with 5% Horse Serum (Invitrogen), 20 ng/ml EGF (Peprotech), 10 μg/ml insulin (Sigma), 100 ng/ml cholera toxin, 0.5 μg/ml hydrocortisone, 50U/ml penicillin and 50 μg/ml streptomycin

(Invitrogen) [64]. All stable cell lines, MCF-10A pBabe (control cell) and MCF-10A pBabe-NeuT (NeuT cell), were produced by retroviral infection of MCF-10A cells followed by treatment with the selectable marker puromycin, as previously described [64].

3.2.2 Cell suspension preparation

For TSM sensor measurement, a cell suspension (7×105 cells/ml) was prepared by treating control or NeuT cells with 0.25% trypsin, centrifuging, and resuspending the cell pellets in serum-free media [DMEM/F12 (Invitrogen Co.), 20ng/ml epidermal growth factor (EGF), 10 μg/ml insulin, 100 ng/ml cholera toxin, 0.5 μg/ml hydrocortisone, 50 units/ml penicillin and 50 μg/ml streptomycin]. For the inhibition of integrin binding with firbronectin (FN), MCF-10A pBabe cells were treated with 1mM soluble Gly-Arg-Gly-Asp-Ser (GRGDS; Sigma Chemical Co.) for 10 min at 37 ºC (GRGDS-treated control cells).

3.2.3 Surface treatment

For coating the surface, both the TSM sensor and the gold coated substrate were immersed in a 5 μg/ml FN solution (Sigma Chemical Co.) for 1 hour at room temperature. After the treatment, the solution was aspirated and the surface was rinsed with PBS two times.

3.2.4 TSM sensor measurement

The TSM sensor device and the measurement system have been described previously (21). Briefly, the sensor device was made by building a chamber, having an inner diameter of 9.2mm and a height of 1.8 mm, on an AT-cut quartz crystal (f0=5MHz, International Crystal Manufacturing, Oklahoma City, OK). The sensor devices were then placed in a humidified incubator (37ºC, 5% CO2) and connected to a network analyzer through a custom-designed micro-wave switch. After temperature equilibrium was established, 130μl of cell suspension (37ºC, 7×105 cells/ml) was gently pipetted into the chamber. The sensor devices were operated at the 3rd overtone harmonic frequency (f3=15 MHz), and the resistance changes (ΔR) at the resonance frequency were recorded once every minute. ΔR reports the energy

dissipation due to the change of mechanical properties (density and viscosity) during the cell adhesion process on the sensor surface.

3.2.5 Optical measurement of cell spread area

For optical imaging, the opaque sensor was replaed with a transparent gold substrate (gold layer thickness: 30nm), prepared by depositing gold onto a circular glass coverslip (diameter: 15mm) with an e-beam evaporator. At specific time points during the incubation (37ºC, 5% CO2), images were taken from randomly chosen locations using an inverted microscope, and then the cells were returned to the incubator. The cell spread area was calculated with NIH ImageJ program.

3.2.6 Spinning disk adhesion assay

A custom made spinning disk cell detachment device similar to that of Garcia was used to determine cell adhesion strength[26] (See appendix 2.). The transparent gold coated glass coverslip (dia: 40mm) was prepared as described above and mounted on the disk (dia: 40mm). A cell suspension (37ºC, 7×105 cells/ml) was placed on the substrate and incubated (37ºC, 5% CO2) for 5 min. Then, the disk was installed on the rotating shaft, and the chamber was filled with PBS (37ºC). The installation time (less than 1 min) was strictly controlled. The rotating speed was increased over 30 seconds to 2000 rpm (control and NeuT cells) and 1000 rpm (GRGDS-treated control cells) and then kept constant for 5 minutes before decreasing to zero over 30 sec. The substrate was transferred to the inverted light microscope, and photomicrographs were taken at defined positions along the diameter. The shear stress increases linearly with radial position. The shear stress at which 50% of adherent cells were removed ($\tau_{50\%}$) was used as the measure of adhesion strength.

3.2.7 Western blot

Cell lysates were prepared as previously described[64]. Briefly, cell lysates were prepared in RIPA buffer (150 mM NaCL, 1% NP-40, 0.5% DOC, 50 mM TrisHCL at pH 8, 0.1% SDS, 10% glycerol, 5 mM EDTA, 20 mM NaF and 1 mM Na3VO4) supplemented with

1 μg/ml each of peptatin, leupeptin, aprotinin, and 200 μg/ml PMSF. Lysates were cleared by centrifugation at 16,000g for 20 min. at 4°C and analyzed by SDS-PAGE and autoradiography.

3.3 Results

3.3.1 Oncogenic regulation of integrin expression

Its been previously shown that the oncogene Her2/Neu can upregulate α5 integrin expression in mammary epithelial cells[23], We compared the relative amount of α5 integrin in control MCF-10A cells, a normal human immortalized mammary epithelial cell line, with cells stably overexpressing oncogenic version of Her2/Neu (NeuT). Our results confirmed that stable overexpression of the oncogene NeuT induces approximately 2 fold higher protein expression of α5 integrin compared to normal MCF-10A cells (Fig. 3.1).

3.3.2 Microscopic measurement of cell spread area

Phase contrast photomicrographs were taken in order to quantify the spread area at specific time points for the comparison with TSM sensor readings (Fig. 3.2). MCF-10A cells were incubated on FN coated transparent gold substrates, under the same experimental conditions as the TSM sensor measurements. Most NeuT cells were attached and partially spread at the 15 minutes and fully spread after 30 minutes. In contrast, many control cells were still round at 15 minutes, but they continued to spread gradually. GRGDS-treated control cells showed slower spreading than untreated control (Fig. 3.3A).

3.3.3 Comparison of time course of ΔR with cell area

The change in motional resistance, ΔR, is a measure of the viscous loss at the sensor surface. The time course of ΔR was compared with the spread area of cells obtained from the microscopic measurement (Fig. 3.3A). The rate of spreading of MCF-10A cells was increased as a result of NeuT overexpression, compared to control cells. Conversely, blocking the specific binding of integrins with soluble GRGDS treatment of control cells decreased the rate of spreading. In addition, the effects of modulating integrins were also clearly seen in the

time-dependent changes in ΔR. The three experimental conditions resulted in qualitative and quantitative differences in the real time spreading behavior as detected by the TSM sensor. NeuT cells showed faster initial increase in ΔR compared to control cells. GRGDS-treated control cells significantly attenuated the ΔR response compared to untreated control cells. The long-term adhesion profile showed that after the initial sharp increase to a maximum value, the ΔR for NeuT cells plateaued and even decreased slightly at later time points. In contrast, the control cells showed gradual increases throughout the experimental period (20 hours) (Fig. 3.3B). Though GRGDS treatment attenuated the response throughout the experimental period, the profile was similar to the untreated cells, with a continuously increasing signal. Thus, alteration of integrin expression or function can be qualitative and quantitative measured by the TSM sensor.

3.3.4 Correlation of TSM sensor readings with cell spread area

Relating the cell area to the changes in ΔR at each time point revealed three distinct phases in the spreading process (Fig. 3.4). Before the cells spread beyond the projected area of their spherical shape in suspension, there was an increase in ΔR without a detectable area change as the cells form initial adhesions and flatten on the surface, but before spreading. Then there was a period of spreading in which the ΔR was linearly related to the change in spread area. The same number of cells was used for each condition, so the spread area per cell is also indicative of the area fraction of the sensor surface occupied by cells. As the cells approach their maximum spread area, there is a period in which ΔR continues to change at approximately constant cell area, indicating a change in mechanical properties. The slope of ΔA/ΔR in the linear region was similar for all three conditions. However, the magnitude of ΔR for a given area varied owing to the differences in the initial adhesion phase.

3.3.5 Correlation of the initial rate of change of ΔR with $\tau_{50\%}$

The integrin mediated adhesivity of cells was investigated with the spinning disk adhesion assay. MCF-10A cells were incubated on the FN coated substrate for 5 minutes, then

exposed to the shear stress generated by the hydrodynamic flow. Photomicrographs of the adherent cells along one diameter of the substrate were taken after the detachment experiment (Fig. 3.5). Adhesion strength was quantified in terms of the shear stress at which 50% of adherent cells became detached, $\tau_{50\%}$ (Fig. 3.6). $\tau_{50\%}$ of NeuT cells was higher than control cells, and GRGDS-treated cells showed the lowest $\tau_{50\%}$. The initial (between 5 min and 10 min) rate of change ΔR, was linearly related to the adhesion strength (Fig. 3.6).

3.4 Discussion

We have investigated the real time changes in interfacial structural properties, as reported by TSM sensor, during the cell adhesion process to determine mechanical and adhesive properties of cells relevant to their functional phenotype. By independently assessing spread area and adhesion strength, we were able to relate the characteristics of the sensor response to the cell adhesion process.

By comparing spread area with sensor readings, we were able to identify three phases in the spreading process (Table 3.1). After the initial attachment, the cell-substrate contact area increases as the cell flattens to conform to the sensor surface (Phase I). Next, the cell spreads beyond the projected area of the unspread spherical cell. During this phase, the ΔR of the sensor increases linearly with the area (Phase II). After the cells reach their maximum spread area, there are further changes in ΔR that represent changes in mechanical properties at the sensor surface (Phase III).

The initial adhesive interaction between the cells and the substrate are driven by the specific integrin-mediated adhesion. We expected the NeuT transformed cells to have greater affinity for the FN coated substratum correlating with the enhanced expression of $\alpha5\beta1$ integrin[65]. Indeed, these cells showed greater detachment strength in the quantitative cell adhesion assay. The approximately 2 fold higher expression of $\alpha5$ in NeuT overexpressing cells correlates well with the measured increase in adhesion strength. Differences in adhesion

strength for normal and transformed MCF-10A cells as well as normal cells blocked with GRGDS showed a strong correlation with the initial rate of change of ΔR. During this period, the cell-substrate contact area has not increased beyond the projected area of the unspread spherical cell, and conventional light microscopy does not allow a direct measure of the contact area during this phase. The TSM sensor technique reported here provides a method for monitoring the kinetics of cell adhesion during this phase. Furthermore, the correlation between the adhesion kinetics reported by the TSM sensor and the adhesion strength provides more quantitative information on the adhesive interaction than contact area alone.

In Phase II, the cells spread beyond the projected area of the unspread, spherical cell. The relationship between ΔR and ΔA in phase II is linear with an offset, ΔR_o. Even though the affinity modulation of α5β1 integrin, either by increased expression or by blocking with soluble GRGDS, induced differences in the size of ΔR at the given spread area, the rate of increase of ΔR with respect to ΔA was the same for all conditions (Fig. 3.4). Because ΔR is related to the mechanical properties of the material in contact with the sensor surface, the linear relationship indicates that the mechanical properties of the cells are constant during this phase of the spreading process and that the change in ΔR is due to the increase in area fraction occupied by the cells as they spread. Though we cannot relate the ΔR changes to contact area during this very early phase of contact, a hypothetical extrapolation of the linear region to zero contact area has a positive ΔR axis-intercept (ΔR_o). The offset in the zero contact area ΔR may indicate the intrinsic adhesivity of the cell. Consistent with the previous results, ΔR_o was greatest for the NeuT overexpressing cells and least for the GRGDS-treated control cells.

When the spread area reached the maximum, ΔR did not maintain the linear relationship with ΔA (Phase III). Instead, ΔR continued to increase at approximately constant cell area indicating a change in mechanical properties. Changes in ΔR during this phase could represent the formation and maturation of focal adhesions, elaboration of cytoskeleton, or a combination thereof.

The change to the malignant phenotype is characterized by interrelated changes in the regulation of proliferation and apoptosis, the expression of integrins, and cell motility. The human mammary epithelial cell model, MCF-10A, used in this study forms normal acinar structures in 3-D gel cultures, that form hollow duct-like structures and recapitulate many architectural features of the glandular epithelium in vivo [66]. MCF-10A cells overexpressing wildtype version of Her2/Neu adopt a premalignant phenotype and disrupts the normal acinar structure by filling the luminal space [66]. Cells overexpressing the oncogenic version of Her2/Neu (NeuT) when placed in 3D culture form highly invasive, disorganized and proliferative structures (S. Caldwell and M. Reginato, unpublished data) with properties similar to invasive breast cancer in vivo. Transformation can also affect the spreading behavior because of the increased adhesivity. In addition, Her2/Neu, in concert with transforming growth factor (TGF)-β, increases the activity of Rac and promotes the motility of MCF-10A cells [67, 68]. We observed well developed lamellipodia in NeuT cells throughout the spreading process, which is consistent with this aspect of Her2 overexpression (Fig. 3.2). Cellular motility is modulated by not only changes in integrin expression, but also other factors. For example, cell stiffness, cytoskeletal dynamics, and contractile properties all modulate migratory behavior in addition to cell substrate adhesion [54, 69].

The continuous, real-time sensor response provides not only cell spreading kinetics, but also intrinsic properties that may help predict migratory and invasive properties of malignant cells. The characteristic sensor response to the attachment and spreading of the two cell types reflects differences in adhesive and structural properties relevant to the functional phenotype. MCF10A pBabe-NeuT cells have rapid spreading with large ΔR, indicating greater adhesion strength on FN. However there is no progressive increase in ΔR, and even a slight decease, after spreading is complete, suggesting no further development of cytoskeletal structure or focal adhesions. MCF 10A pBabe-NeuT cells whose amount of α5 integrins were reduced by siRNA knock-down assay followed the same profile of untreated NeuT cells, but with smaller

size of ΔR (Fig. 3.7A). In contrast, normal cells have less rapid spreading response, but ΔR continued to increase after cells are fully spread. Simple modulation of adhesivity by blocking with soluble GRGDS decreased the initial adhesion response in ΔR, but did not alter long term increase in ΔR, characteristic of the normal response. These characteristic profiles were also observed in the adhesion of NeuT cells on matrigel, though the values of ΔR were reduced relative to their responses on FN (Fig 3.7B). Tumorigenic MDA-MB-231 cells on both FN and matrigel surfaces showed the same profile of NeuT cells on FN (Fig. 3.7C).

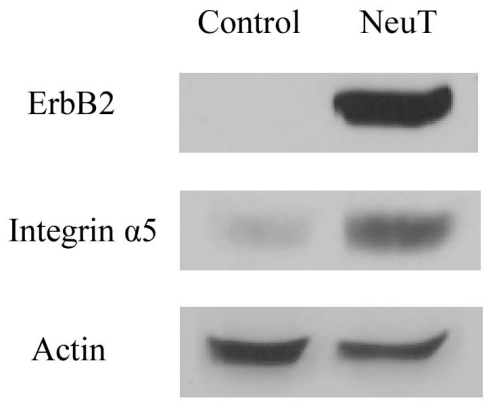

Figure 3.1 MCF-10A cells overexpressing ErbB2 (NeuT) up-regulate integrin α5 expression. Lysates from cells expressing vector alone (pBabe) or ErbB2 (pBabe-NeuT) were collected and proteins were analyzed by immunoblotting with antibodies to ErbB2, integrin α5 and actin.

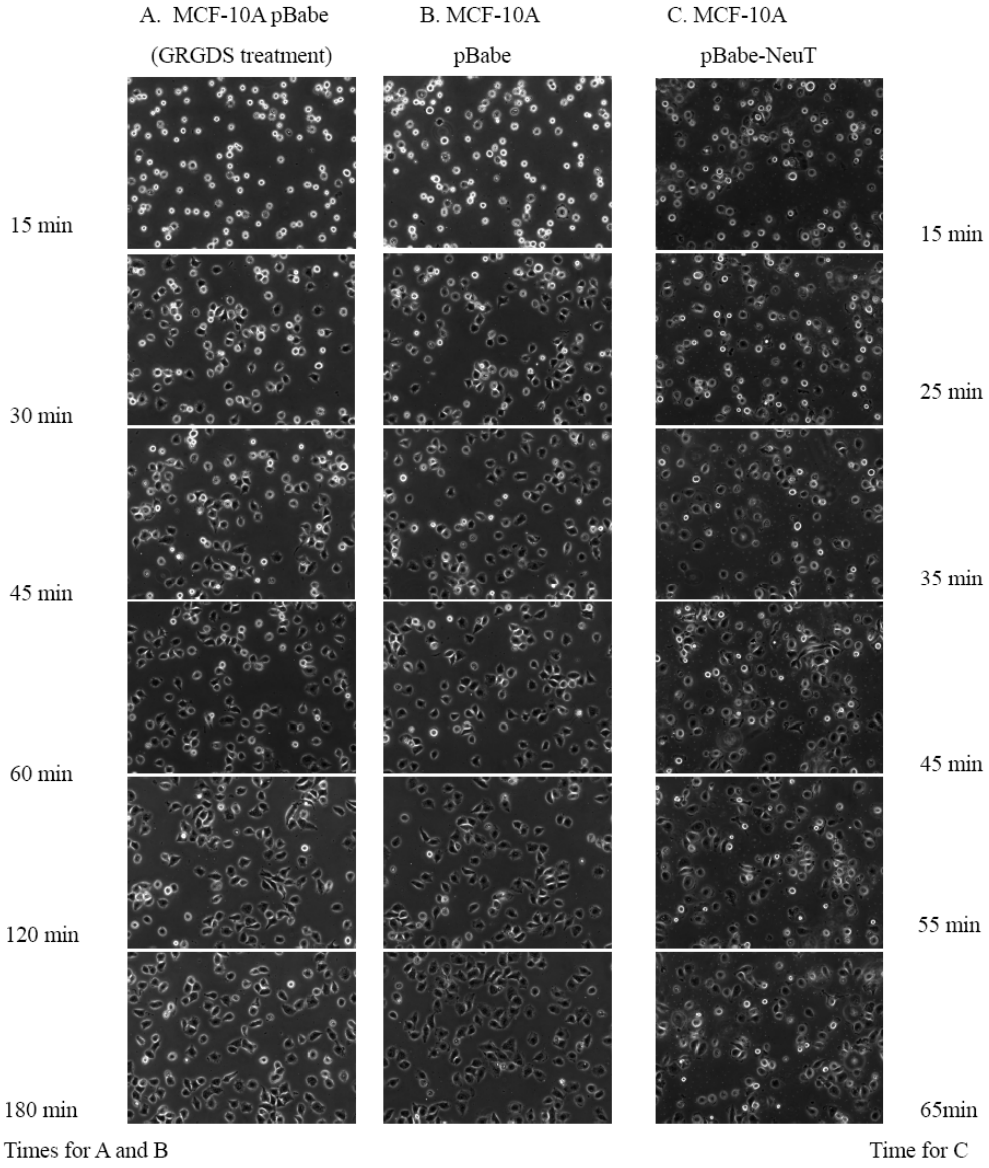
A. MCF-10A pBabe
(GRGDS treatment)
B. MCF-10A
pBabe
C. MCF-10A
pBabe-NeuT
15 min
30 min
45 min
60 min
120 min
180 min
15 min
25 min
35 min
45 min
55 min
65min
Times for A and B
Time for C

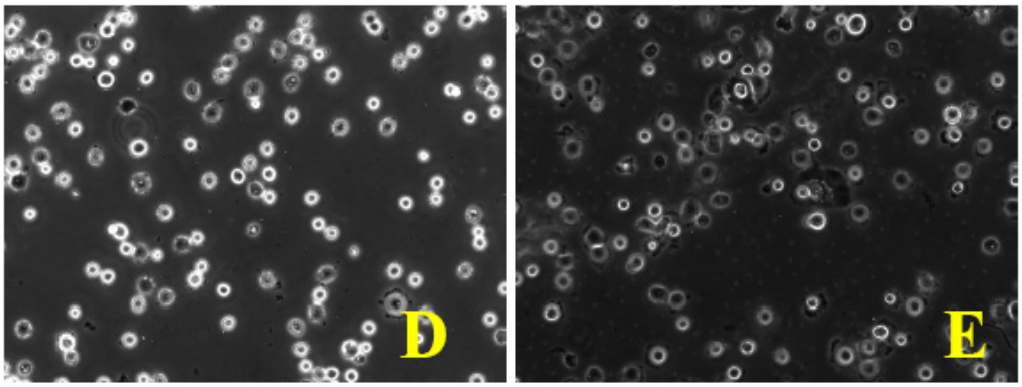
D
E

Figure 3.2 Real time phase contrast photomicrographs of MCF-10A cell spreading on FN surface. The suspended cells (GRGDS, control and NeuT) were allowed to adhere on FN in serum free media. Even though GRGDS cells spread slower than control cells, they showed the similar morphology. NeuT cells showed distinct cell spreading behavior to the rest. While GRGDS and control cells kept their spreading gradually from the round shape, NeuT cells were quite well attached and showed fast spreading with well developed lamellipodia through out the spreading process. The size of each photo is $600\times450\mu m^2$. Enlarged photos of control and NeuT cells at 15 min incubation were shown in D and E respectively.

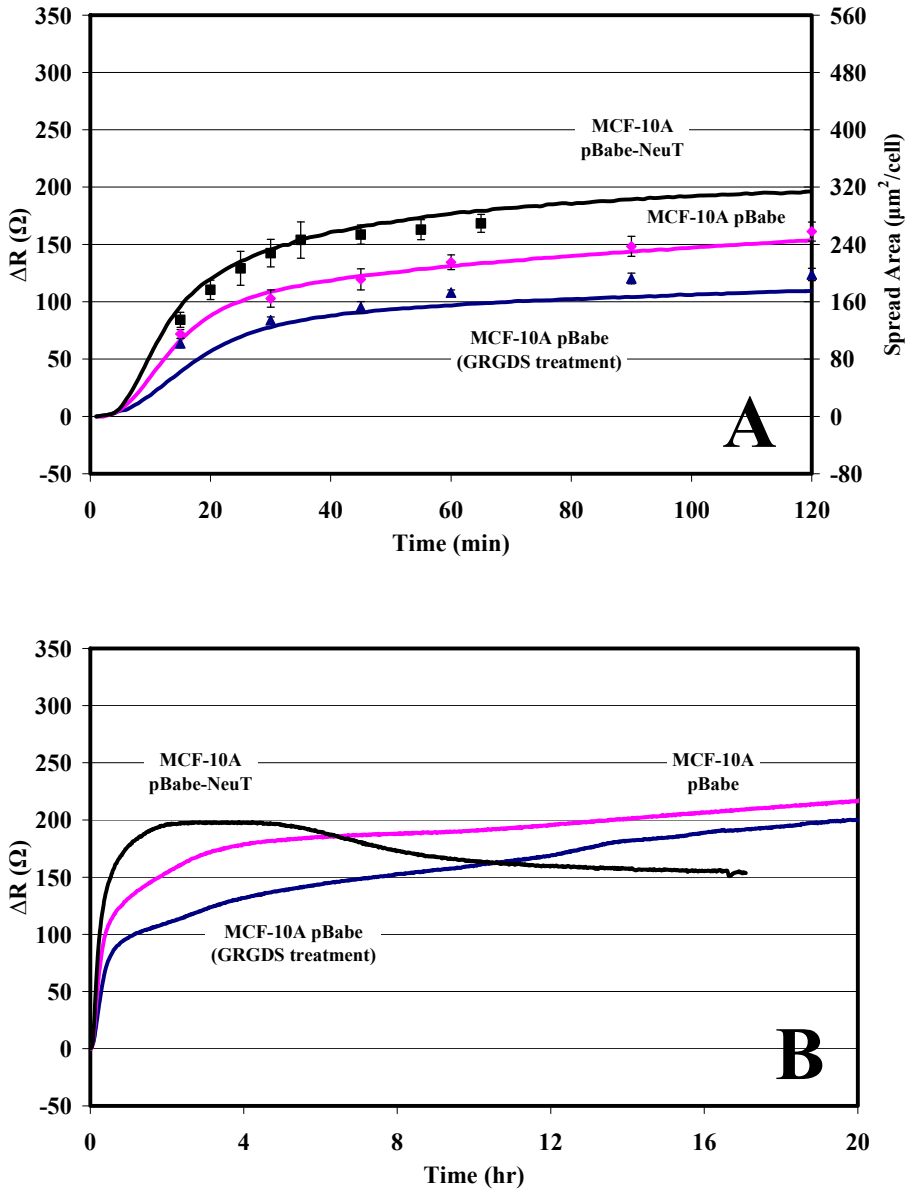

Figure 3.3 A: The comparison of ΔR and ΔA during the MCF-10A cell spreading on FN surface. The spreading area (NeuT cells: ■, Control cells: ♦, GRGDS-treated control cells: ▲), calculated from the image processing, were depicted along with the TSM sensor response (Solid lines). This comparison clear demonstrates that ΔR represents the real time spreading process. A significant difference between ΔA and ΔR was observed in the early spreading of GRGDS cells, which is due to the overestimation of real contact area. B: Long-term time course of ΔR due to the MCF-10A cell adhesion on FN surface. NeuT cells have rapid ΔR increase to the maximum in 2 hours, which may indicate the completion of spreading. There is no progressive increase in ΔR, and even a slight decease, suggesting no further development of cytoskeletal structure or focal adhesions. In contrast, normal cells have less rapid spreading response, but ΔR continued to increase after cells are fully spread.

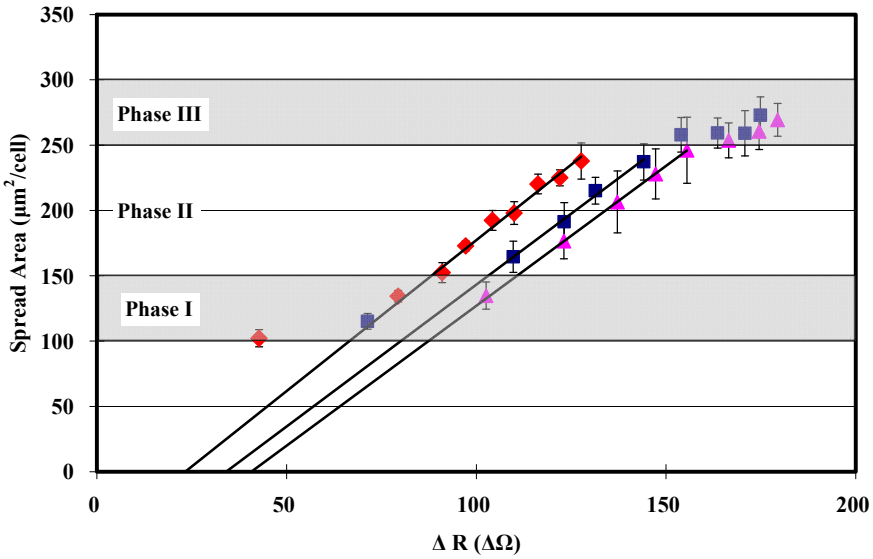

Figure 3.4 Correlation of the spread area and TSM sensor reading (ΔR) for GRGDS cells(♦), control cells(■), NeuT cells(▲). The correlation demonstrates that the cell spreading process consists of three distinct phases. Phase I represents the initial attachment from sedimentation to flattening and the further spreading is in phase II, which is characterized by the linear relationship between ΔR and ΔA. The curve fitted lines from the points in this region have similar slopes and different ΔR axis-intercepts (ΔR_o). When the cell spreading turns into phase III, the linear relationship does not persist. The error bar represents standard deviation (n=12)

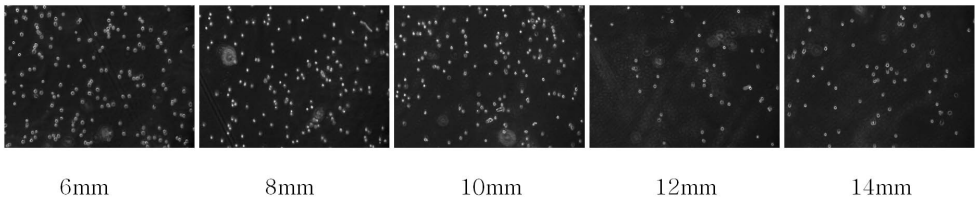

Figure 3.5 Photomicrographs of remaining NeuT cells on the substrate after spinning disk detachment. The distance at which 50% of adherent cells were removed was determined from these sequential images and the corresponding shear stress ($\tau_{50\%}$) was calculated from their linear relationship. Since hydrodynamic force was designed to remove cells in the stage of very initial attachment. $\tau_{50\%}$ indicates the intrinsic adhesivity of the cell. The numbers indicate the distance from the center of the round substrate. The size of each photo is 600×450μm2.

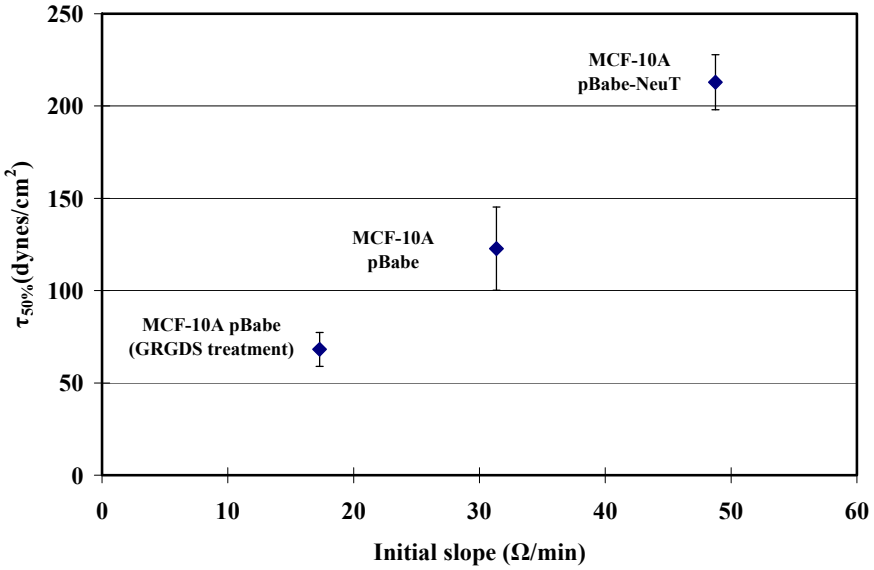

Figure 3.6 Correlation of $\tau_{50\%}$ with the initial slope of ΔR. The initial increasing slope of ΔR was calculated from the difference of ΔR values at 5 and 10min, which is the similar time frame with the spinning disk detachment assay for $\tau_{50\%}$. The result demonstrates that the initial slope is linearly proportional to $\tau_{50\%}$.

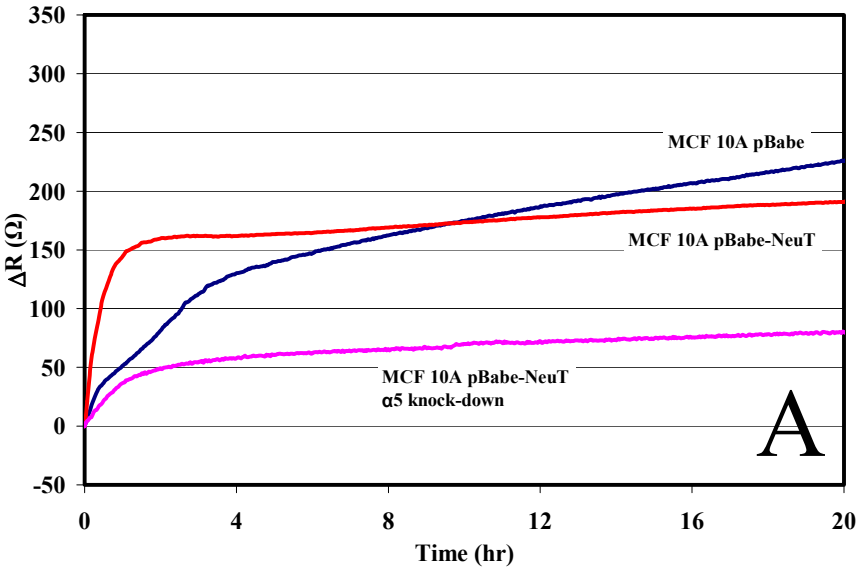
350
300
250
200
150
100
50
0
-50
ΔR (Ω)
0
4
8
12
16
20
Time (hr)
MCF 10A pBabe
MCF 10A pBabe-NeuT
MCF 10A pBabe-NeuT
α5 knock-down
A

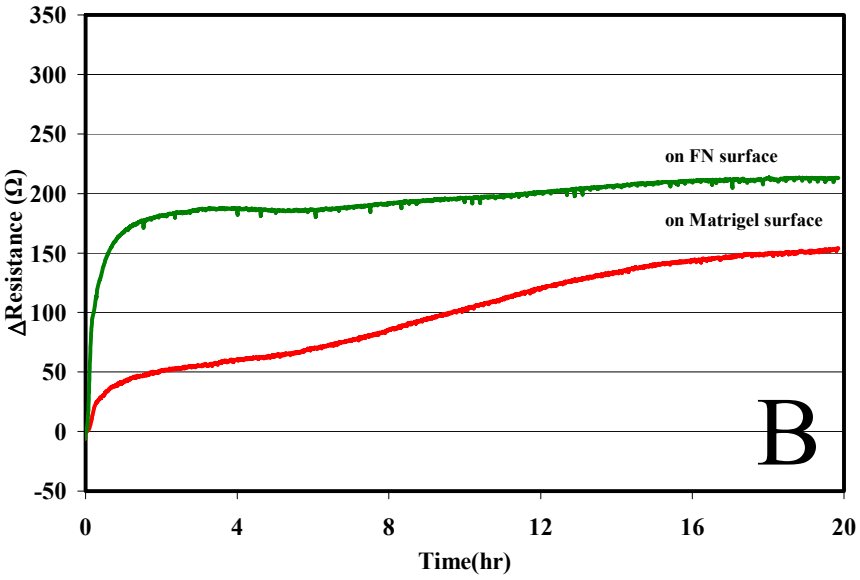
350
300
250
200
150
100
50
0
-50
ΔResistance (Ω)
0
4
8
12
16
20
Time(hr)
on FN surface
on Matrigel surface
B

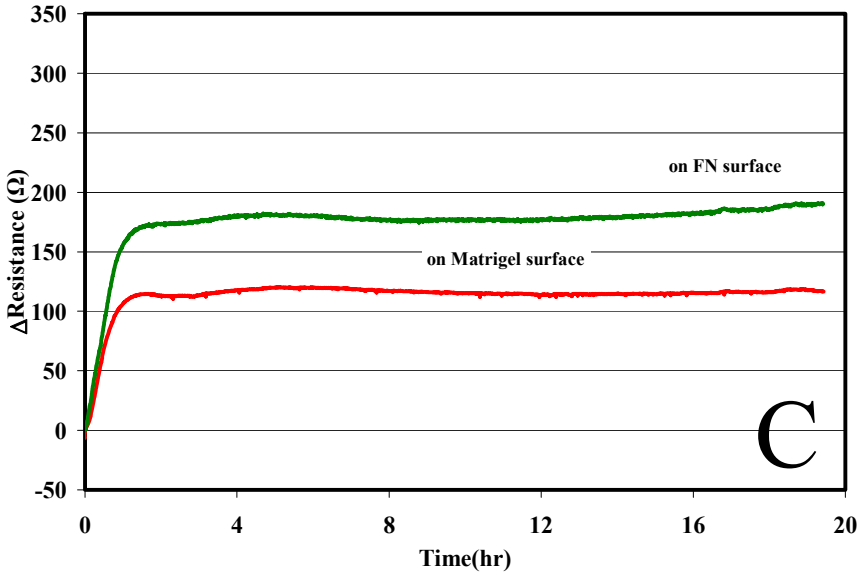

Figure 3.7 The characteristic sensor response to the attachment and spreading may reflects differences in adhesive properties relevant to the functional phenotype. A) MCF10A pBabe-NeuT cells have rapid spreading with large ΔR, indicating greater adhesion strength on FN. Normal cells have less rapid spreading response, but ΔR continued the gradual increase. α5 integrin knock-down NeuT cells showed the same profile of NeuT cells, but has reduced size of ΔR. B) The time course of ΔR of NeuT cells on matrigel surface is similar to that of untreated controls. C) MDA-MB-231 cells followed the same profiles on both FN and matrigel surface.

Table 3.1 Three phases of cell spreading process

	Phase I	Phase II	Phase III	
Cell shape	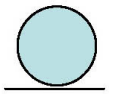	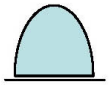		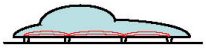
Events	**Initial attachment**	**Flattening**	**Fully spreading**	**Structural reorganization (CSK, FA)**

CHAPTER 4

CELL STIFFNESS AND DEFORMABILITY

4.1 Introduction

In previous decades, mechanical properties of a living cell, which are inherent and/or externally imposed, have been studied to elucidate cellular functions and states. Mechanical properties of both adherent and suspended cells are closely related to the cytoskeleton, which is the polymeric network of structural filaments including actin, intermediate filament and microtubule [70]. Especially, cortical actin-filaments, which form a dense network close to the cell membrane, resist the external forces in the front line, determining the cellular stiffness and deformability [71]. Since the actin-filament network formation is the central indicator for morphological changes due to various cellular events, such as adhesion, migration and transformation, the assessment of mechanical properties provides us with substantial information about the progression of these events. For example, alterations of stiffness and deformability have been observed in cancer cells and abnormal blood cells, which are attributed to the reduction of actins and the change of cytoskeleton structural bindings, respectively [72, 73].

For the measurement of mechanical properties and deformability, many techniques have been developed [74, 75], such as a micropipette aspiration [76, 77], an optical tweezer [78], an optical stretcher [73], a microplate compression [79]. Recently, a nano-indentation using an atomic force microscope (AFM) has been widely used [80, 81] because of the convenience of the experiment and the simplicity of the theoretical analysis. However, this nano-indentation assay contains excessive assumptions and only reports regional elastic properties [82]. Also, it has limitations in providing the deformability which is influenced by both mechanical properties and cell shape.

In this study, the elastic moduli (Young's moduli) of normal and oncogene expressing cells were estimated and the effect of the cell stiffness on the cellular initial adhesion was demonstrated in terms of the TSM sensor measurement. For this, we used a custom made cantilever with a polystyrene hemisphere attached at the end and deformed a spherical cell with its flat surface. The deformation of the spherical cell according to the compressive force was obtained from the force curve and then, Young's modulus was estimated by applying the Hertz contact theory. The cell deformation was computer-simulated with a finite element (FE) analysis and was compared with the experimental data. Also, for reducing the stiffness of normal cells, the cell suspension was treated with the cytochalasin D (CD), which disrupts the actin-filament network [83].

4.2 Material and methods

4.2.1 Cell culture and CD treatment

Normal and oncogene (Her2/neu) expressing MCF10A cells were cultured and cell suspension were prepared as described in 3.2. For the disruption of the actin filaments, CD stock solution in DMSO was added in normal cell suspension at the final concentration of 0.5μM and incubated for 15 min at 37 ºC.

4.2.2 Atomic Force Microscopy (AFM)

A polystyrene hemisphere (diameter of the flat surface: 40μm) was attached at the end of the V-shape silicon nitride cantilever (k: 0.12N/m) (Veeco, Santa Barbara, CA) (Fig. 4.1). The flat surface of the hemisphere was ensured to be parallel to the substrate. The hemisphere cantilever was calibrated with the commercial standard probe (k: 2.625N/m, Veeco) and its spring constant was determined to be 0.1828 N/m. The prepared cell suspension was gently placed on the glass slide installed on the atomic force microscope (Bioscope; Veeco), which was mounted on the inverted fluorescence microscope (TE2000; Nikon, Melville, N.Y.). In order to enhance the experimental reproducibility, the center of the hemisphere was placed on

the top of the cell and the cantilever was engaged and disengaged periodically (0.5Hz, loading rate: 4μm/sec) at room temperature. Loading force curve data was stored for the further analysis. Ten sets (cells) of the experiment were conducted for each sample, i.e. NeuT cells, control cells and CD-treated cells. The size of a spherical cell was measured with a phase contrast microscope and determined to be 15μm in diameter. This value was used in both theoretical and FE analysis.

4.2.3 Theoretical Background and Data analysis

The compressive force (F) and the deformation of the cell (d) can be obtained from the deflection of the cantilever (δ) and its difference from the movement of the cantilever base (Z), shown as[80]

$$F = k\delta\,, \tag{4.1}$$

$$d = Z - \delta\,, \tag{4.2}$$

where k is the spring constant of the cantilever. Since the compressive force and the cellular deformation depend on the deflection of the cantilever, the determination of the deflection due to the contact with the cell, i.e. the contact point from the force curve, is essential for the overall analysis. In our study, the slope of the deflection in the unit movement of the cantilever base was calculated and the point that shows the abrupt slope change was chosen as a contact point in the force curve.

In order to evaluate Young's modulus of the cell, it was assumed that a spherical cell is an incompressible, homogeneous, and isotropic elastic solid. Since a spherical cell was compressed between two rigid parallel plates, one half of the cell body was considered for the theoretical calculations (Fig. 4.2). Young's moduli between 2% and 10% deformation were calculated because the measurement uncertainty under 2% could cause significant experimental errors (Data not shown) and it was reported that the Hertz contact theory doesn't match with the experimental data over 10% deformation [84]. Young's modulus was

calculated by using the Hertz contact theory in which the deformation of an elastic sphere by a rigid surface can be expressed as [85]

$$F = \frac{4}{3}\frac{E\sqrt{R_o}}{(1-\upsilon^2)}d^{3/2}, \tag{4.3}$$

where E is Young's modulus, R_o is the radius of the cell and ν is Poison's ratio (ν=0.5).

For the hyperelastic solid analysis, Mooney-Rivlin (MR) solid model has been widely used for the soft-tissue and its strain energy density function (W) is described [86] as

$$W = C_{10}(I_1 - 3) + C_{01}(I_2 - 3), \tag{4.4}$$

where C_{10} and C_{01} are constants and I_1 and I_2 are the first and the second invariants, which are commonly used with

$$\left.\begin{aligned} I_1 &= \lambda_1^2 + \lambda_2^2 + \lambda_3^2 \\ I_2 &= \lambda_1^2\lambda_2^2 + \lambda_2^2\lambda_3^2 + \lambda_3^2\lambda_1^2 \end{aligned}\right\} \tag{4.5}$$

where, λs are principal stretch ratios.

Since the cell body was assumed as incompressible ($\lambda_1\lambda_2\lambda_3=1$) and axisymmetric ($\lambda_2=\lambda_3$) , the eq. (4.4) becomes

$$W = C_{10}(\lambda_1^2 + 2\lambda_1^{-1}) + C_{01}(2\lambda_1^2 + \lambda_1^{-2}), \tag{4.6}$$

and the corresponding stress is

$$\sigma_1 = C_{10}(2\lambda_1^2 + 2\lambda_1^{-1}) + C_{01}(2\lambda_1 + 2\lambda_1^{-2}). \tag{4.7}$$

This provides the expression for the stress in terms of the strain of hyperelastic materials.

4.2.4 Finite Element (FE) Analysis

The axisymmetric FE models were constructed using the commercial program, ABAQUS (ver. 6.5, ABAQUS, Inc., Providence, RI). The hemisphere's flat surface and glass slide were modeled as rigid bodies, having surface contacts with the cell body (Fig. 4.3). The average Young's modulus calculated from the Hertz contact model was assigned to FE model

and the reaction forces acting on the rigid surface were obtained in terms of the displacement of the rigid surface, i.e. the deformation of the cell. The reaction forces were compared with the AFM experiment data.

For the strain energy density function describing a hyperelastic solid (eq. (4.6)), MR FE model was made and the reaction force on the flat surface according to the cell deformation was calculated. The constants (C_{10} and C_{01}) that have the least mean squared error between forces of the AFM experiment and the FE simulation were chosen.

4.3 Results

4.3.1 Young's modulus and deformability of a spherical cell

Young's modulus of a spherical cell was calculated (Fig. 4.4) by applying the Hertz contact theory to the relationship between the compressive force and the cell deformation (Fig. 4.5), which was calculated from the force curve (Fig. 4.5 inset). For better understanding, several representative points from 2% to 10% of cell deformation were selected for depicting the compressive forces and Young's moduli. The applied forces gradually increased along with the deformation of the cells and those of control cells showed bigger values than NeuT overexpressing cells for the same amount of the deformation. The differences in the calculated Young's modulus can be characterized by two features. First, Control cells have bigger average Young's modulus than NeuT cells (2.95kPa±0.34 vs. 1.09kPa±0.36), which implies that the control cells need larger compressive forces than NeuT cells to be deformed by the same amount. Second, Young's modulus of control cells showed a gradual increase, making larger difference with those of NeuT cells, which are similar values throughout the compression. CD treated cell showed same characteristic behaviors with NeuT cells. Also, the deformability, defined as the ratio of the cell deformation (d) to the cell radius (R_o) at a given compressive force, can be assessed from the force-deformation curve (Fig. 4.5). For example,

when the 3nN of the compressive force is applied, deformabilities of control and NeuT cells were 5% and 9%, respectively.

4.3.2 Validation of Hertz contact theory with FE analysis

For the validation of Young's moduli calculated from the Hertz contact theory, FE model was constructed and reaction forces were compared with the AFM experiment data (Fig. 4.5). The comparison result demonstrated that FE analysis data are in good agreement with those of the AFM experiment indicating that the application of the Hertz contact theory provides reasonable values of Young's modulus. The control cells showed larger difference between the experiment and the FE analysis than both NeuT cells and CD treated cells.

4.3.3 Mooney-Rivlin hyperelastic properties of a spherical cell

For the hyperelastic analysis, the force-deformation curve of MR model consistent with AFM experiment results were obtained from the FE simulation by varying the constants of C_{10} and C_{01} (Fig. 4.5). Corresponding constants which have the minimum mean squared error were -2.7 kPa and 3.0 kPa, respectively. While the stress-strain curve (δ-ε) obtained from the strain energy density function (W) showed similar values in a small deformation range ($d>6\%$) with that of Hertz contact theory, the differences between values becomes larger as the deformation increases (Fig. 4.6).

4.3.4 The effect of cell stiffness on the initial attachment of cells

The reduction of the cell stiffness by disrupting the cytoskeleton with CD treatment caused the change in the time course of ΔR. The control cells showed typical response described in Chapter 3, but CD treated cell showed slightly higher values in the initial stage (<2.5min) than control cells and gradually increased. The adhesion of CD treated cells maintained smaller ΔR at all later times.

4.4 Discussion

AFM, allowing the physical contact with the biological sample under the physiological condition, has been widely used not only for rastering the surface, but also for estimating mechanical properties. For mechanical properties, the sample is usually indented with a pyramid or a sphere AFM tip and Young's modulus is calculated by applying the Hertz contact theory which describes the deformation of two elastic contacting spheres. However, this nano-indentation assay may not be sufficient to evaluate the accurate Young's modulus because of several over-assumptions stated by others, such as a nonlinearity of force-deformation due to the increase of the indenting contact area [82]. Moreover, since the indentation reports the regional deformation near the surface, the mechanical behavior may not reflect the property of the entire body. Thus, this cannot provide the direct information about the deformability. To overcome this limitation, a tipless cantilever was introduced for compressing a spherical sample, but this also contains problematic issues. The cell sample tends to be compressed by two non-parallel flat surfaces and the V-shape cantilever may not cover the deformed surface completely. The experimental method proposed in this study, i.e. compressing a spherical cell with a hemisphere cantilever, can provide Young's modulus as well as deformability while avoiding limitations mentioned above. A wide range of Young's moduli of adherent endothelial cell lines (1~10kPa) has been reported from the AFM indentation work [87-90]. Considering that the suspended spherical cell is softer than the adherent cell, our result (E: 2.2 ~ 4.0 kPa) seems to be reasonable. However, these values are higher than those from a micropipette aspiration (0.1~1kPa) [91] and a flexible microplate (0.3kPa)[79].

AFM experiment results demonstrated that the compressive force showed a gradual increase in terms of the cell deformation rather than a straight increase (Fig. 4.5). This non-linearity is attributed to geometrical and material specialties of a round cell. Unlike the typical compression testing specimen, the contact area of a spherical cell with the flat surface linearly increases with the deformation and the reaction forces are distributed in the concentric contour

pattern. A cell body consists of various proteins, organelles, and filamentous elements. Especially, cortical actin-filament layer underneath the cell membrane significantly affects on cellular mechanical properties, which is evidenced by the observation that the disruption of actin-filaments by CD treatment caused cells to be more compliant and close to the homogeneity. Theoretically, the total reaction force of the homogeneous elastic sphere contacting the rigid flat surface is a function of the deformation with the power 3/2 (eq. (4.3)) [84]. However, the compressive forces from the AFM experiment were not well curve-fitted with the power 3/2, which arises from the fact that a cell shows complex mechanical properties rather than homogenous elastic solid properties. The comparison of experimental data with a FE analysis strongly demonstrated that the Hertz contact theory is acceptable to describe the overall mechanical behavior of the cell under the compression (Fig. 4.5). The observation that Young's modulus became larger as the deformation increased leads to the consideration of the hyperelastic model (Fig. 4.4). The FE simulation showed that the hyperelastic model can describe the cell deformation better than linear elastic (Hookean) solid model. The stress-strain curve obtained from the MR hyperelastic strain energy density function is non-linear. The comparison of stress-strain curves indicates that the stress causing a unit deformation in MR solid model is greater than that of Hertz contact theory and the difference become larger as the strain increases. Typically polymers, such as rubber, have been described well by MR constitutive law. Cross-linked polymer chains allow an easy deformation at the initial stress, but generate greater resistance to the stress as being stretched to the cross-linked points. This property can be enhanced by giving more cross-link points, such as disulfide bonds in vulcanized rubber. The observation that disruption of the cross-linked actin filament network with the CD treatment made the cell lose the non-linearity can be explained with the same concept. Also, the analysis may indicate that actin filament of NeuT cells are disrupted by Her2 oncogene signaling, which decreases cellular stiffness.

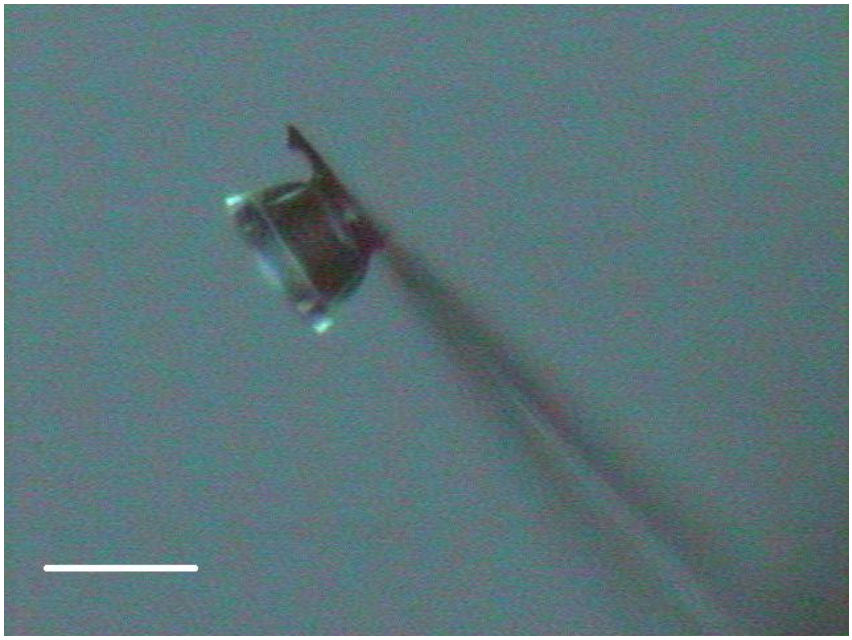

Figure 4.1 A polystyrene hemisphere was attached at the end of a silicone nitride cantilever. A spherical polystyrene bead was half melted on a flat glass slide and the AFM cantilever was engaged on the top of the formed hemisphere with UV glue, followed by the UV light cure. The spring constant was determined to be 0.1828N/m using a commercial calibration probe. The bar is 40μm.

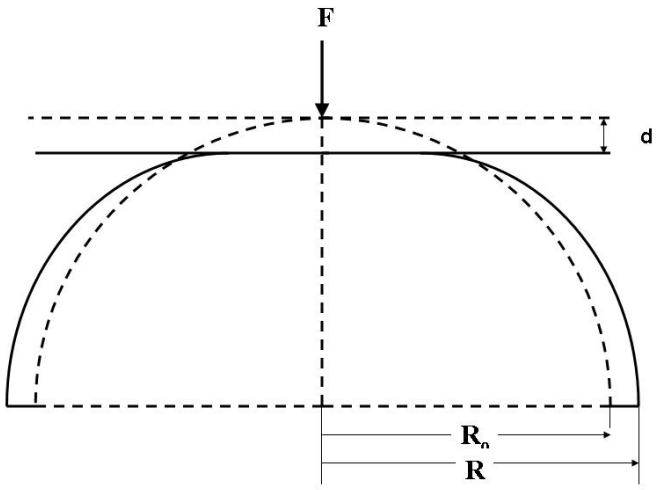

Figure 4.2 The deformation of one half of a spherical solid compressed by a rigid plate. Hertz contact theory describes the relationship between the compressive force (F), deformation (d), and elastic modulus (Young's modulus) as shown in eq. (4.3). The compressive force is the function of the deformation with the power 3/2.

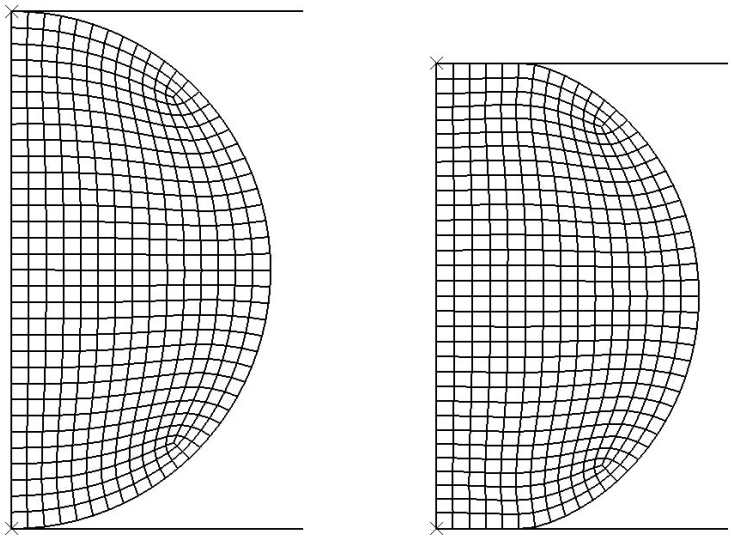

Figure 4.3 Axisymmetric FE model and its deformation under the compression by two rigid parallel plate. The average Young's modulus calculated from the Hertz contact model was assigned to FE model and the reaction forces acting on the rigid surface wre obtained in terms of the displacement of the rigid surface.

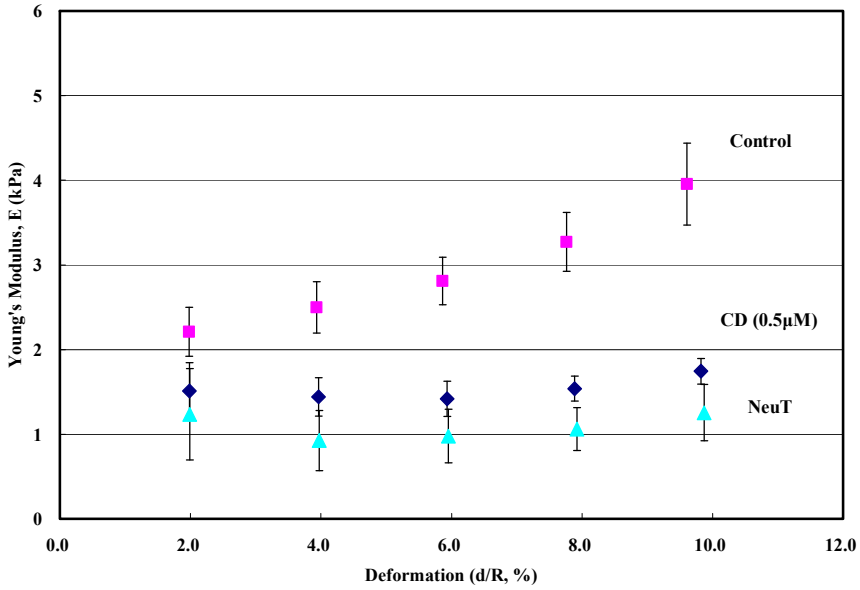

Figure 4.4 Comparison of Young's moduli calculated with Hertz contact theory (■: Control cells, ◆: CD treated cells and ▲: NeuT overexpressing cells). For better understanding, several representative points from 2% to 10% of cell deformation were selected for depicting the Young's modulus. Control cells showed bigger averaged values than NeuT cells and while NeuT and CD treated cells maintained relatively constant values according to the deformation, those of control cells gradually increase. Error bar indicates the standard deviation (n=10).

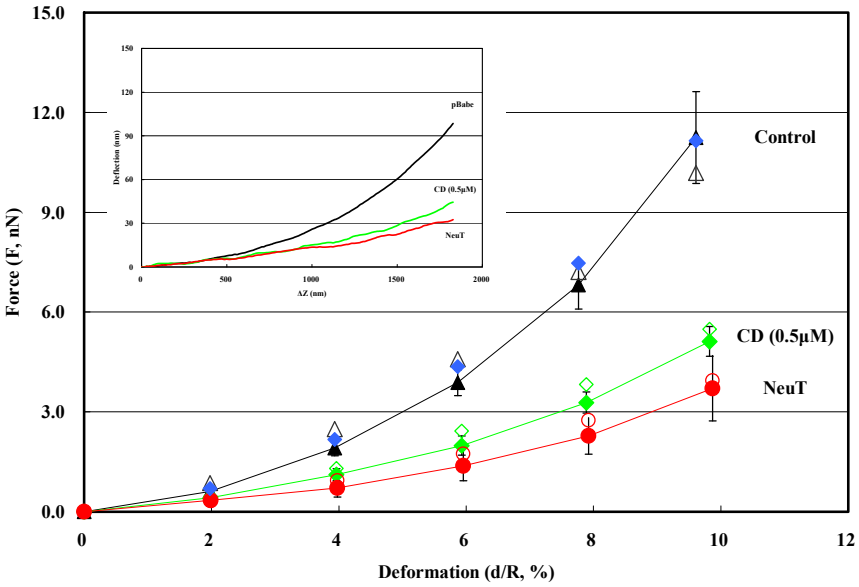

Figure 4.5 The relationship between the compressive force and the cell deformation from the experiments (filled symbols and solid lines) and FE model simulations (hollow symbols for Hookean solid model and ◆ for Mooney-Rivlin solid model). Representative force curves were shown in the inset. Error bar indicates the standard deviation (n=10).

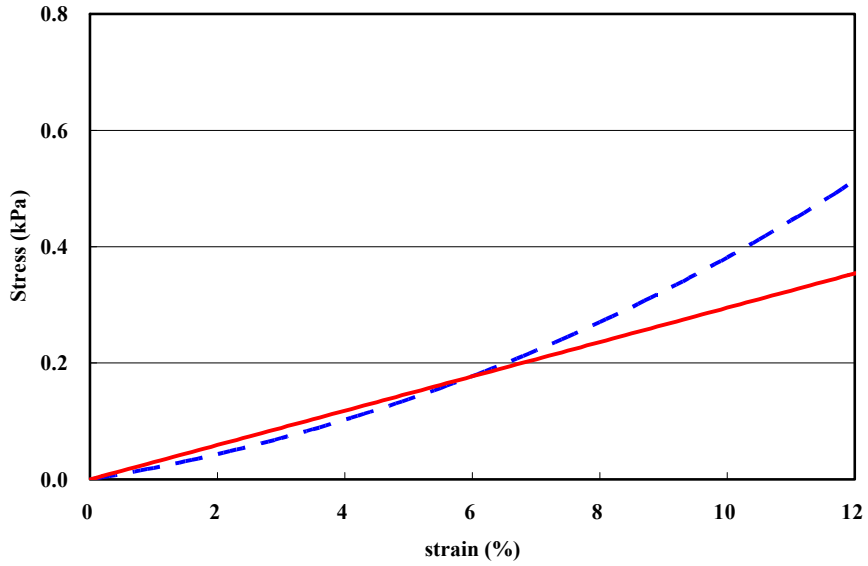

Figure 4.6 Stress and strain curves of the elastic solid model (solid line) and MR hyperelastic solid model (dashed line). While solid model has linear stress-strain curve (δ-ε), MR hyperelastic solid model showed non-linear relationship.

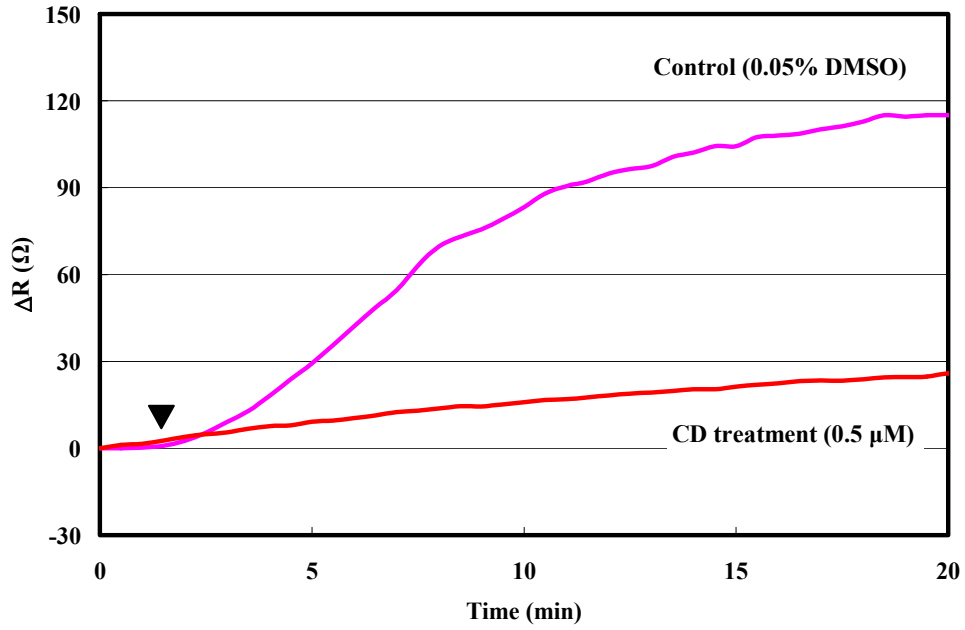

Figure 4.7 The influence of the cell stiffness on the initial attachment of cells. The adhesion of control cells showed the typical time course of ΔR, but that of CD treated cell showed slightly higher values in the initial stage (<2.5min), noted by ▼, and gradually increased. This may indicate that CD treated cells deform faster and generate smaller sensor signals than control cells.

CHAPTER 5

CONCLUSIONS AND FUTURE WORK

5.1 Conclusions

This study provides a foundation for using TSM sensors to analyze the adhesion and spreading of cells in real time. Results of this study showed that the cell sedimentation process was influenced by electrostatic interactions with the substrate as indicated by change in the delay time on PDL surface. The initial attachment and spreading process were determined by integrin binding, and their kinetics and strength could be characterized by the slope and the size of ΔR at primary plateau, respectively. HSPG contributed the long term adhesion, but did not affect the initial adhesion kinetics. Independent assessment of cell spread area and adhesion strength has allowed us to assign physical meaning to the characteristics of the sensor response in the various phases of the adhesion process. The initial slope of ΔR is linearly related to the intrinsic adhesivity of cells. In the second phase, ΔR is linearly related to the spread area of the cell. The comparison of the adhesion of MCF-10A pBabe and pBabe-NeuT showed that the activation of ErbB2 produced quantitative differences in cell adhesivity on FN consistent with the up-regulation of α5β1 integrin. Also, ErbB2 overexpressing cells showed higher deformability and faster initial attachment. Taken together, these results demonstrate the utility of the TSM sensor technique for monitoring the kinetics of cell adhesion in real time. We have shown that the technique is sensitive enough to detect the effects of specific molecular interventions that can be used to characterize the adhesive state of a cell or to decipher the molecular constituents of the adhesive interactions with natural or artificial substrates. The interpretation of the real time changes in ΔR in terms of the intrinsic adhesivity and the cell spreading process enhance the importance and usefulness of the TSM

sensor measurement system in the cell adhesion study, especially, in analyzing the adhesive characteristics and their effects on the phenotypic variations of cells on specific ECM proteins.

5.2 Future work

The experimental and analytical platform for assessing the cell-surface interactions described in the current study can be used to investigate several research topics.

5.2.1 Structural changes of cells

The sensor response to the adhesion of various cell lines showed different patterns in the long terms adhesion, as well as the initial adhesion. Since ΔR reports the energy dissipation due to the mechanical property changes in the sensor surface, the sensor reading change, maintaining the constant spread area, indicates structural changes both in the cell-surface and in the cell body. The most possible events that affect the sensor response in the long term adhesion can be the maturation of cytoskeleton and FA formation. We expect that their development will decrease the slope ($\Delta R/\Delta A$) of phase III. For the correlation with sensor response, they can be visualized can be quantified either measuring the intensity or/and the area.

5.2.2. Functional phenotype of tumorigenic cells.

The abnormal activation of oncogene regulates the level of specific integrins and the corresponding intrinsic adhesivity change determines the overall cell behavior including spreading kinetics as we have shown in this study. Here, we suggest an investigation elucidating the relationship between the intrinsic adhesivity and the motility, which is one of the functional phenotype of tumorigenic cells. The invasive tumorigenic cells are characterized by the high motility, which is governed by the cell-surface interaction cytoskeleton dynamics. We hypothesize that the migratory speed of cells are inversely related

to the intrinsic adhesivity. The level of integrins can be modulated by various methods, such as siRNA knock-down technique.

5.2.3 Transformation of cells

The transformation of normal cells into tumorigenic cells accompanies sequential changes in both cell adhesivity and cell structure. We expected that these changes show the signature in the time course of ΔR, which reveals characteristics of oncogenes and/or cancer cell lines. The time course of transformation of cells can be obtained by introducing oncogene with retrovial infection to normal cells. By analyzing the sensor response to the transformation process, we might assess not only detail variations in adhesivity and adhesion but also transformation kinetics.

LIST OF REFERENCES

1. Arnaout, M.A., S.L. Goodman, and J.P. Xiong, *Structure and mechanics of integrin-based cell adhesion.* Curr Opin Cell Biol, 2007. **19**(5): p. 495-507.
2. Geiger, B., et al., *Transmembrane crosstalk between the extracellular matrix--cytoskeleton crosstalk.* Nat Rev Mol Cell Biol, 2001. **2**(11): p. 793-805.
3. DeMali, K.A., K. Wennerberg, and K. Burridge, *Integrin signaling to the actin cytoskeleton.* Curr Opin Cell Biol, 2003. **15**(5): p. 572-82.
4. Sivakumar, P., et al., *New insights into extracellular matrix assembly and reorganization from dynamic imaging of extracellular matrix proteins in living osteoblasts.* J Cell Sci, 2006. **119**(Pt 7): p. 1350-60.
5. Ruoslahti, E. and M.D. Pierschbacher, *Arg-Gly-Asp: a versatile cell recognition signal.* Cell, 1986. **44**(4): p. 517-8.
6. Schoenwaelder, S.M. and K. Burridge, *Bidirectional signaling between the cytoskeleton and integrins.* Curr Opin Cell Biol, 1999. **11**(2): p. 274-86.
7. Hynes, R.O., *Integrins: bidirectional, allosteric signaling machines.* Cell, 2002. **110**(6): p. 673-87.
8. Hughes, P.E. and M. Pfaff, *Integrin affinity modulation.* Trends Cell Biol, 1998. **8**(9): p. 359-64.
9. Comoglio, P.M., C. Boccaccio, and L. Trusolino, *Interactions between growth factor receptors and adhesion molecules: breaking the rules.* Curr Opin Cell Biol, 2003. **15**(5): p. 565-71.
10. Gambaletta, D., et al., *Cooperative signaling between alpha(6)beta(4) integrin and ErbB-2 receptor is required to promote phosphatidylinositol 3-kinase-dependent invasion.* J Biol Chem, 2000. **275**(14): p. 10604-10.
11. Yamada, K.M. and S. Even-Ram, *Integrin regulation of growth factor receptors.* Nat Cell Biol, 2002. **4**(4): p. E75-6.
12. Price, L.S., et al., *Activation of Rac and Cdc42 by integrins mediates cell spreading.* Mol Biol Cell, 1998. **9**(7): p. 1863-71.
13. Borisy, G.G. and T.M. Svitkina, *Actin machinery: pushing the envelope.* Curr Opin Cell Biol, 2000. **12**(1): p. 104-12.
14. Miki, H., et al., *IRSp53 is an essential intermediate between Rac and WAVE in the regulation of membrane ruffling.* Nature, 2000. **408**(6813): p. 732-5.
15. Cavalcanti-Adam, E.A., et al., *Cell spreading and focal adhesion dynamics are regulated by spacing of integrin ligands.* Biophys J, 2007. **92**(8): p. 2964-74.
16. Reinhart-King, C.A., M. Dembo, and D.A. Hammer, *The dynamics and mechanics of endothelial cell spreading.* Biophys J, 2005. **89**(1): p. 676-89.
17. Dubin-Thaler, B.J., et al., *Nanometer analysis of cell spreading on matrix-coated surfaces reveals two distinct cell states and STEPs.* Biophys J, 2004. **86**(3): p. 1794-806.
18. Mercurio, A.M., I. Rabinovitz, and L.M. Shaw, *The alpha 6 beta 4 integrin and epithelial cell migration.* Curr Opin Cell Biol, 2001. **13**(5): p. 541-5.

19. Guo, W., et al., *Beta 4 integrin amplifies ErbB2 signaling to promote mammary tumorigenesis.* Cell, 2006. **126**(3): p. 489-502.
20. Di Fiore, P.P., et al., *erbB-2 is a potent oncogene when overexpressed in NIH/3T3 cells.* Science, 1987. **237**(4811): p. 178-82.
21. Slamon, D.J., et al., *Studies of the HER-2/neu proto-oncogene in human breast and ovarian cancer.* Science, 1989. **244**(4905): p. 707-12.
22. Slamon, D.J., et al., *Human breast cancer: correlation of relapse and survival with amplification of the HER-2/neu oncogene.* Science, 1987. **235**(4785): p. 177-82.
23. Spangenberg, C., et al., *ERBB2-mediated transcriptional up-regulation of the alpha5beta1 integrin fibronectin receptor promotes tumor cell survival under adverse conditions.* Cancer Res, 2006. **66**(7): p. 3715-25.
24. Nauman, E.A., et al., *Quantitative assessment of steady and pulsatile flow fields in a parallel plate flow chamber.* Ann Biomed Eng, 1999. **27**(2): p. 194-9.
25. Reyes, C.D. and A.J. Garcia, *A centrifugation cell adhesion assay for high-throughput screening of biomaterial surfaces.* J Biomed Mater Res A, 2003. **67**(1): p. 328-33.
26. Garcia, A.J., P. Ducheyne, and D. Boettiger, *Quantification of cell adhesion using a spinning disc device and application to surface-reactive materials.* Biomaterials, 1997. **18**(16): p. 1091-8.
27. Roberts, C., Chen, C.S., Mrksich, M., Martichonok, V., Ingber, D.E., Whitesides,G.M. , *Using mixed self-assembled monolayers presenting RGD and (EG)3OH groups to characterize long-term attachment of bovine capillary endothelial cells to surfaces.* J. Am. Chem. Soc. , 1998. **120**: p. 6548-6555.
28. Cavic, B.A., G.L. Hayward, and M. Thompson, *Acoustic waves and the study of biochemical macromolecules and cells at the sensor-liquid interface.* Analyst, 1999. **124**(10): p. 1405-20.
29. Redepenning, J., et al., *Osteoblast attachment monitored with a quartz crystal microbalance.* Anal Chem, 1993. **65**(23): p. 3378-81.
30. Gryte, D.M., M.D. Ward, and W.S. Hu, *Real-time measurement of anchorage-dependent cell adhesion using a quartz crystal microbalance.* Biotechnol Prog, 1993. **9**(1): p. 105-8.
31. Janshoff, A., et al., *Double-mode impedance analysis of epithelial cell monolayers cultured on shear wave resonators.* Eur Biophys J, 1996. **25**(2): p. 93-103.
32. Olivier, L.A., Truskey, G.A., *A numerical analysis of forces exerted by laminar flow on spreading cells in a parallel plate flow chamber assay.* Biotechnol. Bioeng., 1993. **42**: p. 963-973.
33. Moussy, F., A.W. Neumann, and W. Zingg, *The force of detachment of endothelial cells from different solid surfaces.* ASAIO Trans, 1990. **36**(3): p. M568-72.
34. Cozens-Roberts, C., J.A. Quinn, and D.A. Lauffenburger, *Receptor-mediated cell attachment and detachment kinetics. II. Experimental model studies with the radial-flow detachment assay.* Biophys J, 1990. **58**(4): p. 857-72.

35. Davies, P.F., A. Robotewskyj, and M.L. Griem, *Endothelial cell adhesion in real time. Measurements in vitro by tandem scanning confocal image analysis.* J Clin Invest, 1993. **91**(6): p. 2640-52.

36. Neyfakh, A.A., Jr., et al., *Visualization of cellular focal contacts using a monoclonal antibody to 80 kD serum protein adsorbed on the substratum.* Exp Cell Res, 1983. **149**(2): p. 387-96.

37. Wegener, J., A. Janshoff, and H.J. Galla, *Cell adhesion monitoring using a quartz crystal microbalance: comparative analysis of different mammalian cell lines.* Eur Biophys J, 1999. **28**(1): p. 26-37.

38. Marx, K.A., et al., *A quartz crystal microbalance cell biosensor: detection of microtubule alterations in living cells at nM nocodazole concentrations.* Biosens Bioelectron, 2001. **16**(9-12): p. 773-82.

39. Li, J., et al., *Monitoring of integrin-mediated adhesion of human ovarian cancer cells to model protein surfaces by quartz crystal resonators: evaluation in the impedance analysis mode.* Biosens Bioelectron, 2005. **20**(7): p. 1333-40.

40. Barbee, K.A., *Changes in surface topography in endothelial monolayers with time at confluence: influence on subcellular shear stress distribution due to flow.* Biochem Cell Biol, 1995. **73**(7-8): p. 501-5.

41.Florian, J.A., et al., *Heparan sulfate proteoglycan is a mechanosensor on endothelial cells.* Circ Res, 2003. **93**(10): p. e136-42.

42. Dull, R.O., et al., *Lung endothelial heparan sulfates mediate cationic peptide-induced barrier dysfunction: a new role for the glycocalyx.* Am J Physiol Lung Cell Mol Physiol, 2003. **285**(5): p. L986-95.

43. Rotsch, C. and M. Radmacher, *Drug-induced changes of cytoskeletal structure and mechanics in fibroblasts: an atomic force microscopy study.* Biophys J, 2000. **78**(1): p. 520-35.

44. Reimhult, E., Hook, F., Kasemo, B., *Intact Vesicle Adsorption and Supported Biomembrane Formation from Vesicles in Solution: Influence of Surface Chemistry, Vesicle Size, Temperature, and Osmotic Pressure.* Langmuir, 2003. **19**(5): p. 1681-1691.

45. Bell, G.I., M. Dembo, and P. Bongrand, *Cell adhesion. Competition between nonspecific repulsion and specific bonding.* Biophys J, 1984. **45**(6): p. 1051-64.

46. Lee, J.H., et al., *Cell behaviour on polymer surfaces with different functional groups.* Biomaterials, 1994. **15**(9): p. 705-11.

47. van Wachem, P.B., et al., *Adhesion of cultured human endothelial cells onto methacrylate polymers with varying surface wettability and charge.* Biomaterials, 1987. **8**(5): p. 323-8.

48. Burridge, K., et al., *Focal adhesions: transmembrane junctions between the extracellular matrix and the cytoskeleton.* Annu Rev Cell Biol, 1988. **4**: p. 487-525.

49. Bernfield, M., et al., *Functions of cell surface heparan sulfate proteoglycans.* Annu Rev Biochem, 1999. **68**: p. 729-77.

50. Carey, D.J., *Syndecans: multifunctional cell-surface co-receptors.* Biochem J, 1997. **327 (Pt 1)**: p. 1-16.
51. Hynes, R.O., *Integrins: a family of cell surface receptors.* Cell, 1987. **48**(4): p. 549-54.
52. van der Flier, A. and A. Sonnenberg, *Function and interactions of integrins.* Cell Tissue Res, 2001. **305**(3): p. 285-98.
53. Burridge, K. and K. Wennerberg, *Rho and Rac take center stage.* Cell, 2004. **116**(2): p. 167-79.
54. DiMilla, P.A., K. Barbee, and D.A. Lauffenburger, *Mathematical model for the effects of adhesion and mechanics on cell migration speed.* Biophys J, 1991. **60**(1): p. 15-37.
55. Hall, A., *Rho GTPases and the actin cytoskeleton.* Science, 1998. **279**(5350): p. 509-14.
56. Palecek, S.P., et al., *Integrin-ligand binding properties govern cell migration speed through cell-substratum adhesiveness.* Nature, 1997. **385**(6616): p. 537-40.
57. Lauffenburger, D.A. and A.F. Horwitz, *Cell migration: a physically integrated molecular process.* Cell, 1996. **84**(3): p. 359-69.
58. Ruoslahti, E., *Fibronectin and its integrin receptors in cancer.* Adv Cancer Res, 1999. **76**: p. 1-20.
59. Moschos, S.J., et al., *Integrins and cancer.* Oncology (Williston Park), 2007. **21**(9 Suppl 3): p. 13-20.
60. Zou, J.X., et al., *Activated SRC oncogene phosphorylates R-ras and suppresses integrin activity.* J Biol Chem, 2002. **277**(3): p. 1824-7.
61. Plantefaber, L.C. and R.O. Hynes, *Changes in integrin receptors on oncogenically transformed cells.* Cell, 1989. **56**(2): p. 281-90.
62. Cuvelier, D., et al., *The universal dynamics of cell spreading.* Curr Biol, 2007. **17**(8): p. 694-9.
63. Hong, S., et al., *Real-time analysis of cell-surface adhesive interactions using thickness shear mode resonator.* Biomaterials, 2006. **27**(34): p. 5813-20.
64. Reginato, M.J., et al., *Integrins and EGFR coordinately regulate the pro-apoptotic protein Bim to prevent anoikis.* Nat Cell Biol, 2003. **5**(8): p. 733-40.
65. Plopper, G.E., et al., *Migration of breast epithelial cells on Laminin-5: differential role of integrins in normal and transformed cell types.* Breast Cancer Res Treat, 1998. **51**(1): p. 57-69.
66. Muthuswamy, S.K., et al., *ErbB2, but not ErbB1, reinitiates proliferation and induces luminal repopulation in epithelial acini.* Nat Cell Biol, 2001. **3**(9): p. 785-92.
67. Ueda, Y., et al., *Overexpression of HER2 (erbB2) in human breast epithelial cells unmasks transforming growth factor beta-induced cell motility.* J Biol Chem, 2004. **279**(23): p. 24505-13.
68. Muraoka, R.S., et al., *Increased malignancy of Neu-induced mammary tumors overexpressing active transforming growth factor beta1.* Mol Cell Biol, 2003. **23**(23): p. 8691-703.
69. Ridley, A.J., et al., *Cell migration: integrating signals from front to back.* Science, 2003. **302**(5651): p. 1704-9.
70. Boal, D.H., *Mechanics of the cell*. 2002, Cambridge, UK ; New York: Cambridge University Press. xiv, 406 p.

71. Satcher, R.L., Jr. and C.F. Dewey, Jr., *Theoretical estimates of mechanical properties of the endothelial cell cytoskeleton.* Biophys J, 1996. **71**(1): p. 109-18.
72. Glenister, F.K., et al., *Contribution of parasite proteins to altered mechanical properties of malaria-infected red blood cells.* Blood, 2002. **99**(3): p. 1060-3.
73. Guck, J., et al., *Optical deformability as an inherent cell marker for testing malignant transformation and metastatic competence.* Biophys J, 2005. **88**(5): p. 3689-98.
74. Cheng, L.Y., *Deformation analyses in cell and developmental biology. Part II--Mechanical experiments on cells.* J Biomech Eng, 1987. **109**(1): p. 18-24.
75. Suresh, S., *Biomechanics and biophysics of cancer cells.* Acta Biomater, 2007. **3**(4): p. 413-38.
76. Evans, E.A., *Bending elastic modulus of red blood cell membrane derived from buckling instability in micropipet aspiration tests.* Biophys J, 1983. **43**(1): p. 27-30.
77. Hochmuth, R.M., *Micropipette aspiration of living cells.* J Biomech, 2000. **33**(1): p. 15-22.
78. Mills, J.P., et al., *Nonlinear elastic and viscoelastic deformation of the human red blood cell with optical tweezers.* Mech Chem Biosyst, 2004. **1**(3): p. 169-80.
79. Caille, N., et al., *Contribution of the nucleus to the mechanical properties of endothelial cells.* J Biomech, 2002. **35**(2): p. 177-87.
80. A-Hassan, E., et al., *Relative microelastic mapping of living cells by atomic force microscopy.* Biophys J, 1998. **74**(3): p. 1564-78.
81. Costa, K.D., *Imaging and probing cell mechanical properties with the atomic force microscope.* Methods Mol Biol, 2006. **319**: p. 331-61.
82. Costa, K.D. and F.C. Yin, *Analysis of indentation: implications for measuring mechanical properties with atomic force microscopy.* J Biomech Eng, 1999. **121**(5): p. 462-71.
83. Cooper, J.A., *Effects of cytochalasin and phalloidin on actin.* J Cell Biol, 1987. **105**(4): p. 1473-8.
84. Liu, K.K., Williams, D. R., Briscoe, B. J., *The large deformation of a single micro-elastomeric sphere.* J. Phys. D: Appl. Phys., 1998. **31**: p. 294-303.
85. Kogut, L. and I. Etsion, *Elastic-Plastic Contact Analysis of a Sphere and a Rigid Flat.* Journal of Applied Mechanics, 2002. **69**(5): p. 657-662.
86. Ogden, R.W., *Non-linear elastic deformations*. Ellis Horwood series in mathematics and its applications. 1984, Chichester New York: E. Horwood ; Halsted Press. xiv, 532 p.
87. Haga, H., et al., *Elasticity mapping of living fibroblasts by AFM and immunofluorescence observation of the cytoskeleton.* Ultramicroscopy, 2000. **82**(1-4): p. 253-8.
88. Kataoka, N., et al., *Measurements of endothelial cell-to-cell and cell-to-substrate gaps and micromechanical properties of endothelial cells during monocyte adhesion.* Proc Natl Acad Sci U S A, 2002. **99**(24): p. 15638-43.
89. Lekka, M., et al., *Elasticity of normal and cancerous human bladder cells studied by scanning force microscopy.* Eur Biophys J, 1999. **28**(4): p. 312-6.
90. Mathur, A.B., et al., *Endothelial, cardiac muscle and skeletal muscle exhibit different viscous and elastic properties as determined by atomic force microscopy.* J Biomech, 2001. **34**(12): p. 1545-53.

91. Theret, D.P., et al., *The application of a homogeneous half-space model in the analysis of endothelial cell micropipette measurements.* J Biomech Eng, 1988. **110**(3): p. 190-9.

APPENDIX

1. Calculation of the resistance

$$S_{21} = 20\log\left|\frac{100}{100 + Z_T}\right|$$

$$\left|100 + Z_T\right| = 10^{-\left|\frac{S_{21}}{20}\right|} \times 100$$

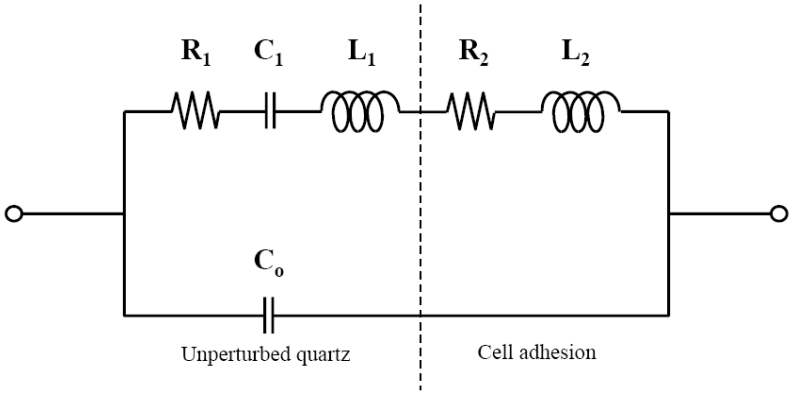

Fig. 1.1 The transmission line model of TSM sensor

From the transmission line model (Fig. 1.1), the admittance is

$$Y_T = \frac{R_m}{R_m{}^2 + \left(\omega L_m - \frac{1}{\omega C_m}\right)^2} + i\left(\omega C_o - \frac{\omega L_m - \frac{1}{\omega C_m}}{R_m{}^2 + \left(\omega L_m - \frac{1}{\omega C_m}\right)^2}\right)$$

Where, $R_m = R_1 + R_2$, $L_m = L_1 + L_2$ and $C_m = C_1$

At resonance frequency (ω_o)

$$\omega L_m - \frac{1}{\omega C_m} = 0$$

$$Z_T = \frac{R_m}{1 + i\omega_o R_m C_o}$$

$$= \frac{R_m\left(1 - i\omega_o R_m C_o\right)}{1 + \omega_o{}^2 R_m{}^2 C_o{}^2}$$

$$\omega_o^{\,2} R_m^{\,2} C_o^{\,2} << 1$$

$$\left| 100 + R_m \left(1 - i\omega_o R_m C_o\right) \right| = k$$

Where, $k = 10^{-\left|\frac{S_{21}}{20}\right|} \times 100$

$$R_m^{\,2} + 200\, R_m + \omega_o^{\,2} R_m^{\,2} C_o^{\,2} + 100^{\,2} - k^{\,2} = 0$$

$$R_m = \frac{-200 \pm \sqrt{200^2 - 4(1 + \omega_o^{\,2} C_o^{\,2})(100^2 - k^2)}}{2(1 + \omega_o^{\,2} C_o^{\,2})}$$

Since $\omega_o^{\,2} C_o^{\,2} \approx 0$

$$R_m = -100 + k$$

For $R_m > 0$

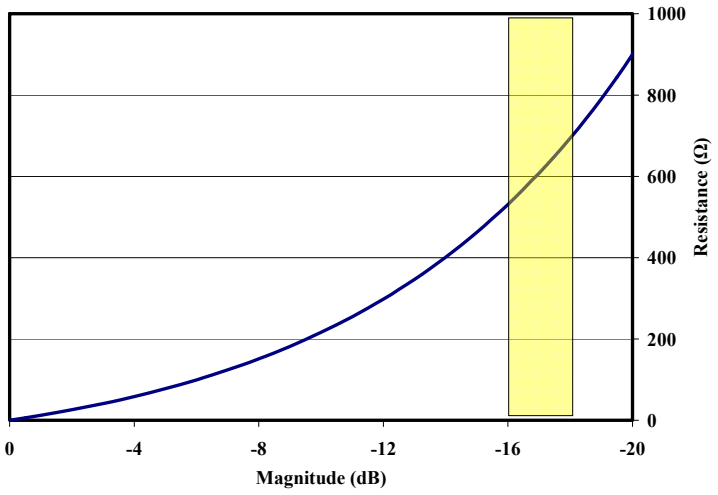

Fig. 1.2 The relation between Mag (dB) and resistance (Ω). The normal sensor response region is noted with yellow box.

2. TSM sensor measurement.

2.1 Preparation of the sensor device

Chambers were built on a TSM sensor by attaching either Teflon cylinders (ID: 11mm) or Viton O-rings (ID 10.8mm) on both sides with silicon glue (Fig. 2.1A). For better electric connections between the TSM sensor and connector, the small amount of silver paint was applied and dried. A round glass slide was prepared to cover the chamber (Fig. 2.1B). The TSM sensor was encaged with a transparent plastic box in order to minimize the experimental error caused by the temperature fluctuation during opening the incubator (Fig. 2.1C). A small hole was made on the lid of the box (Fig. 2.1D) and TSM sensor was installed right below the hole. This hole was used for the aspiration and the inoculation of cell suspension.

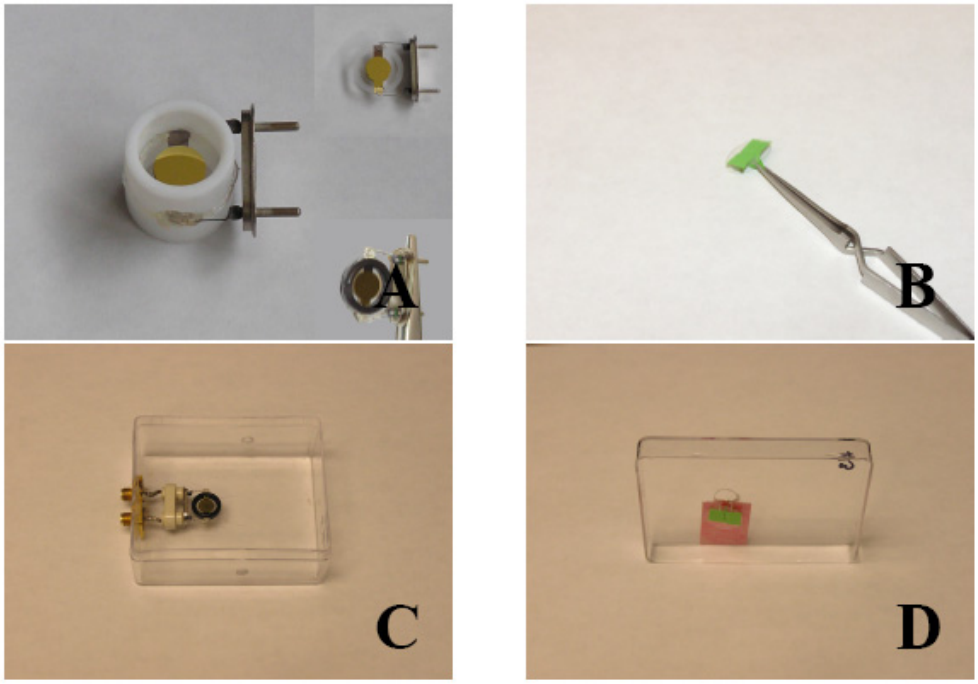

Fig. 2.1 TSM sensor and sensor device

2.2 Experiment protocol

1) Experiment set-up

- The sensor surface is coated with ECM protein (0.5% (v/v) gelatin solution for 30min or 5μg/ml FN solution for 1 hr).
- The surface is rinsed with PBS two times and is immersed with DI water.
- The sensor device (Fig. 2.2A) is placed in the incubator and the sensors are connected to a network analyzer though a micro-wave switch (Fig. 2.2E). A piece of sponge that contains water is placed inside of the box.
- The sensors are allowed to be stabilized and the temperature stability in the box is checked from the sensor response.

2) Cell adhesion measurement. (Experimental steps were shown outside of the incubator for the demonstration)

- Cell suspension is prepared and the vials are placed in the water bath of the incubator for 10 min.
- DI water is aspirated though the hole (Fig. 2.2B).
- 140μl of cell suspension (7×10^5 cells/ml) is placed on the sensor (Fig. 2.2C) and the glass slide is placed on the O-ring (Fig. 2.2D). For the gas exchange the upper part of O-ring was notched (A nail clipper was used to make notches). For Teflon cylinder sensor device, 0.5ml of cell suspension (3.75×10^5 cells/ml) is placed on the sensor. At the same time, the data acquisition program is operated (Fig. 2.2F).

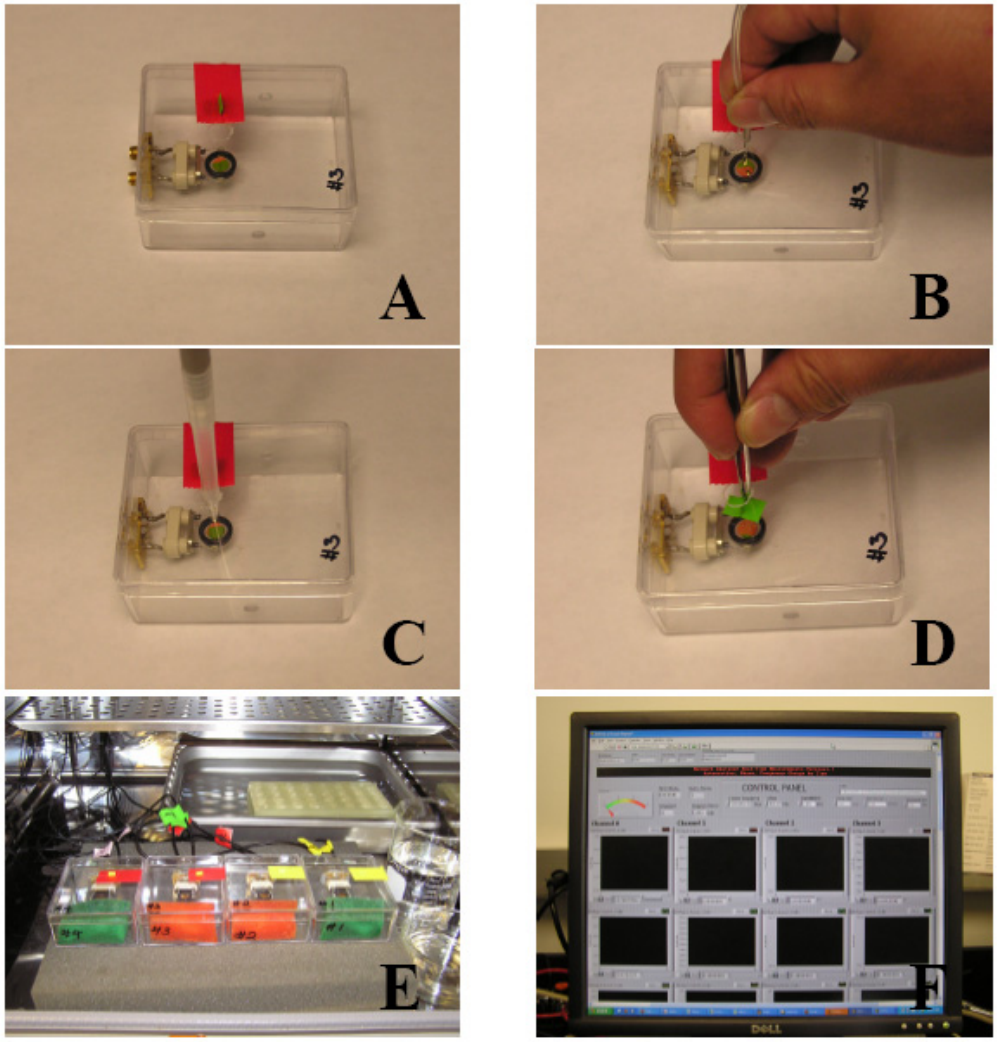

Fig. 2.2 Cell adhesion measurement with TSM sensor.

3. Cell adhesion assay

3.1 Spinning disk apparatus

The hydrodynamic shear force is applied in controllable manner to adherent cells by spinning the disk on which cells are allowed to adhere for certain duration.

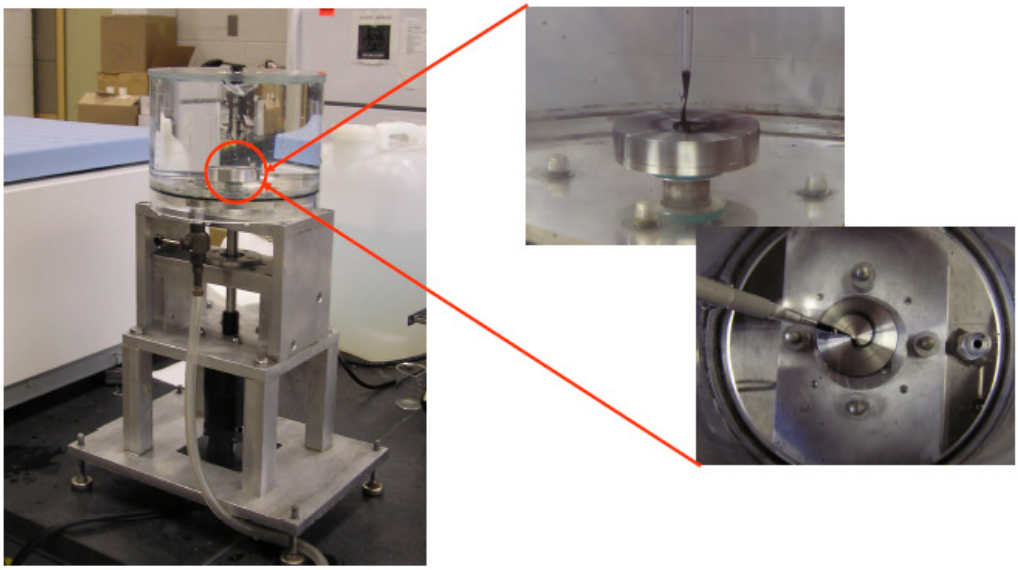

Fig. 3.1 The spinning disk apparatus and diffusion profile.

The shear stress on the surface is linear proportional to the distance from the center (Fig 3.2) and is simply calculated by

$$\tau = 0.8 \cdot r\left(\rho\mu\omega^3\right)^{1/2} \qquad (1)$$

τ = shear stress r = radial dist. from center

μ = fluid viscosity ρ = fluid density

ω = angular velocity

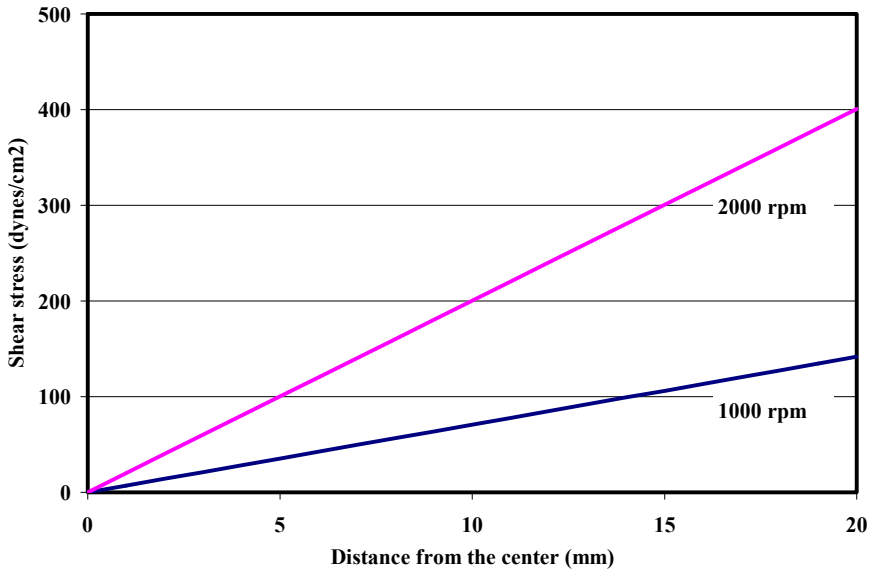

Fig. 3.2 The relationship between the applied shear stress and the distance from the center

3.2 Spinning disk adhesion assay protocol.

1) Preparation of transparent gold coated substrate

- A round glass slide (Dia: 40 mm) is cleaned with 70% alcohol and dried with compressed air (Fig. 3.3Aa).
- The glass slide is installed in the e-beam evaporator (Fig. 3.3B).
- The surface is coated with Cr (thickness: 5nm), followed by being coated with gold (thickness: 30nm) (Fig. 3.3Ab). (For the coating procedure, follow the manufacturer's manual).

2) Preparation of cell sample on the round glass slide.

- The prepared round glass slide is installed on the spinning disk. The round glass can be firmly attached on the surface by the suction cup (Fig. 3.3C, D, E, and F).
- A round mask (Dia: 40 mm) that forms rectangle channel is made from an inert rubber sheet (Fig. 3.3G).
- The mask is placed on the gold coated round glass slide (Fig. 3.3H).

- The surface in the rectangle channel is coated with FN (5μg/ml) for 1hr at room temp.
- The surface is rinsed with PBS two times.
- The prepared cell suspension (cells/ml) is placed in the channel and the top of the mask is covered with glass slide (Fig. 3.3I). (In order to make the sample which has well distributed population of cells, the height of suspension needs to be maintained constant across the channel).

3) Operation of the spinning disk apparatus

- After incubating the sample for the specific time (e.g. 5min) in a humidified, incubator with 5% CO2 in air, the spinning disk is installed on the rotating shaft and the chamber is filled with 37ºC 1X PBS (Fig. 3.3J,K).
- The cover slide and mask are gently removed
- The spinning disk is rotated at specific speed for 5 min with 30 sec increment and 30 sec decrement. The rotation is controlled with specially designed computer program (LabView) (Fig. 3.3M,L).
- When the spinning disc stopped, the glass slide is detached and brought to the inverted microscope. Since the substrate is transparent, the adherent cells can be photographed with a regular inverted microscope (Fig. 3.3N).
- The distance from the center where the adherent cells are reduced over 50% is calculated.

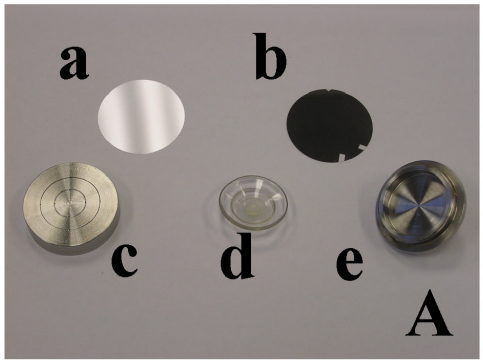
a
b
c
d
e
A


B

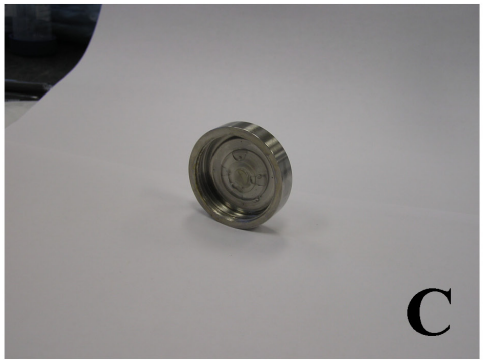
C

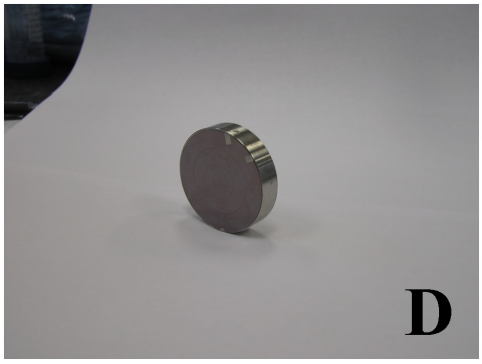
D

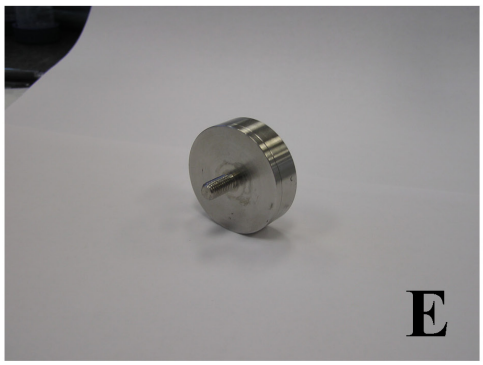
E

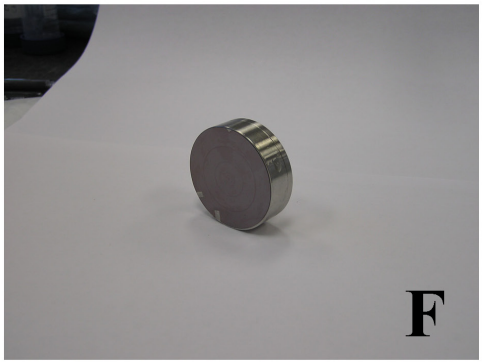
F

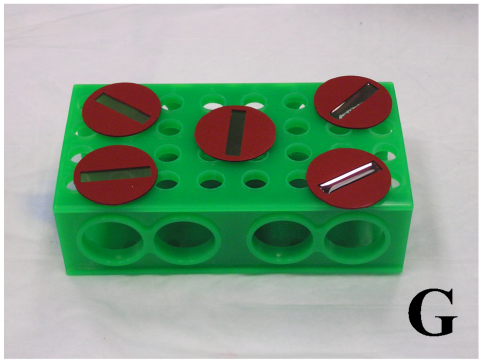
G

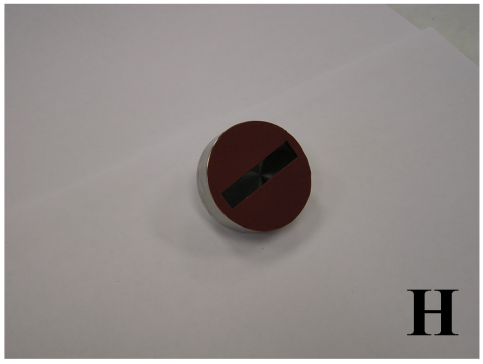
H

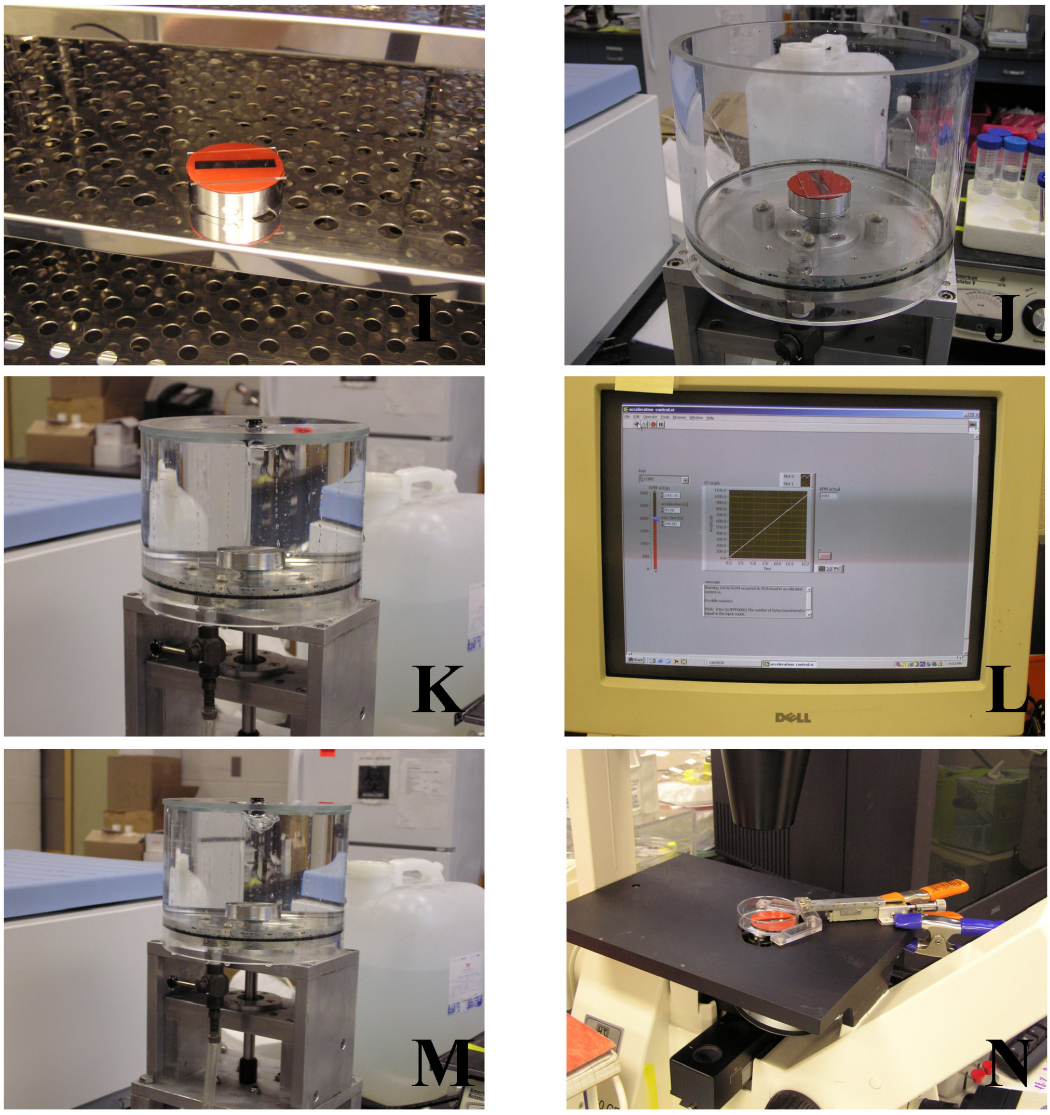

Fig. 3.3 Spinning disk apparatus and its operation.

4. Mechanical testing with AFM.

A hemisphere was made by melting a polystyrene microsphere on a glass slide (Fig. 4.1A) and was attached at the end of silicon nitride cantilever (Fig. 4.1B). For the calibration of the spring constant of the hemisphere cantilever, first we calibrated a regular cantilever with a commercial standard probe (Fig. 4.1C). Then we used the calibrated probe as a standard. Cell suspension was placed on the bare glass and the center of hemisphere was engaged on a single cell (Fig. 4.1D). Then, the force curve was obtained.

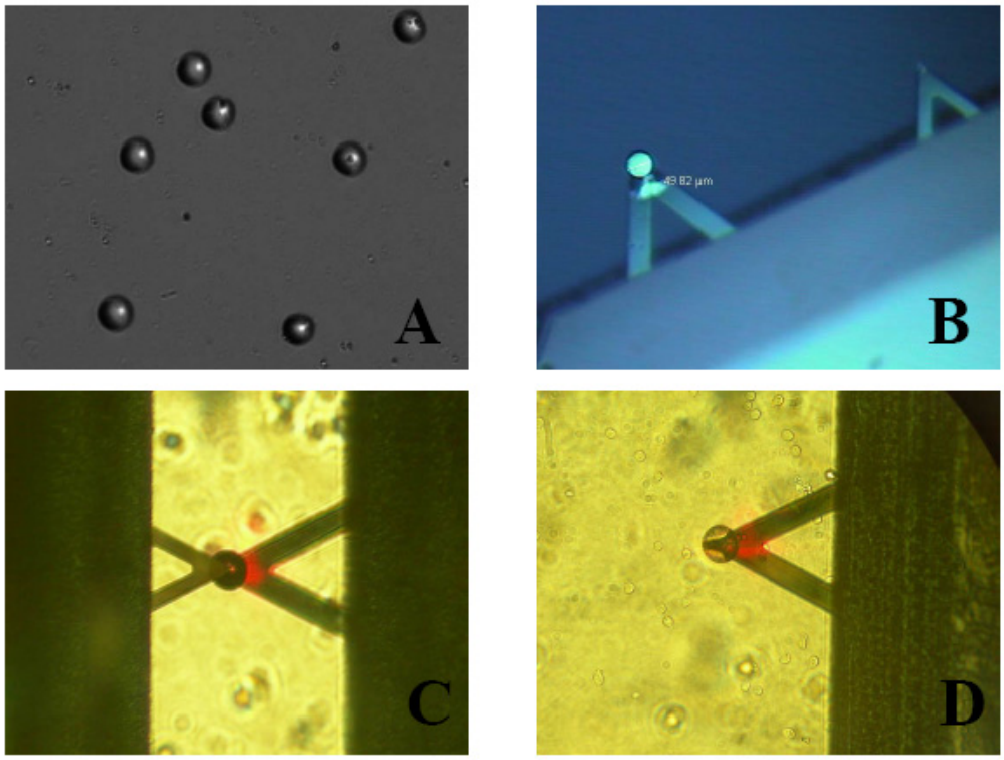

Fig. 4.1 Mechanical testing with AFM

VITA

Soonjin Hong

Education

Ph.D. in Biomedical Engineering, Drexel University, USA 2008

M.S. in Mechanical Engineering, SungKyunKwan University, S. Korea, 1997

B.S. in Mechanical Engineering, SungKyunKwan University, S. Korea, 1995

Employment

Research Engineer (1997 – 2003) Kolon Engineering Co., Ltd., S. Korea

Research Interests

Cell adhesion, Cell-biomaterial interaction, Cell adhesion molecules (CAMs) Integrin-ECM interaction, Biosensors, Biomaterials, Cellular biomechanics, Oncogene expressing phenotype, Cell signaling.

Selected Publications.

- Investigation of the intrinsic adhesivity and spreading of normal and oncogene expressing mammary epithelial cells using thickness shear mode resonator. Hong S et al. (in preparation)
- Mechanical Property of a Whole Cell Measured by Compressing the Spherical Cells with Atomic Force Microscopy. Hong S et al. (in preparation)
- Real time monitoring of the effects of Heparan Sulfate Proteoglycan (HSPG) and surface charge on the cell adhesion process using thickness shear mode (TSM) sensor. Biosens Bioelectron. 2007 Apr 15;22(9-10):2256-60. Ergezen E et al.
- Real-time analysis of cell-surface adhesive interactions using thickness shear mode resonator. Biomaterials. 2006 Dec;27(34):5813-20. Hong S et al.

Selected Presentations.

- BAEC Adhesion Analysis Using Thickness Shear Mode Sensor. 2005 Annual Fall Meeting of the BMES. Sept. 2005 Hong S et al.
- BAEC Adhesion Analysis Using Thickness Shear Mode Sensor. Conf Proc IEEE Eng Med Biol Soc. 2005;1:1047-50. Hong S et al.
- BAEC sedimentation and adhesion analysis using the QCM. 2004 Annual Fall Meeting of the BMES. Oct. 2004. Hong S et al.